Combining Cartilaginous Microtissues Primed Under Altered Oxygen Environments with Melt Electrowritten Meshes to Engineer Scaled-Up Grafts

Nadia Rodriguez [1,2,3], Inês F. Gonçalves [1,2,3], Tom Hodgkinson [4], Fergal J. O'Brien [1,2,3,4] and Daniel J. Kelly [1,2,3,4,*]

[1] Trinity Centre for Biomedical Engineering, Trinity Biomedical Sciences Institute, Trinity College Dublin, Dublin, Ireland.
[2] Department of Mechanical, Manufacturing and Biomedical Engineering, School of Engineering, Trinity College Dublin, Dublin, Ireland.
[3] Advanced Materials and Bioengineering Research Centre (AMBER), Royal College of Surgeons in Ireland and Trinity College Dublin, Dublin, Ireland.
[4] Tissue Engineering Research Group, Department of Anatomy and Regenerative Medicine, Royal College of Surgeons in Ireland, Dublin, Ireland.

* Correspondence: **kellyd9@tcd.ie**

https://doi.org/10.1016/j.bioadv.2025.214680
Received 15 September 2025, Revised 26 November 2025, Accepted 22 December 2025, Available online 25 December 2025, Version of Record 6 January 2026.
Biomaterials Advances 182 (2026) 214680.

Abstract

Current articular cartilage tissue engineering strategies fail to produce grafts that recapitulate the complex zonal composition and organisation of the native tissue. Developmental engineering strategies might overcome such limitations, leading to the generation of more biomimetic grafts by mimicking key steps of normal tissue development. One such approach leverages the capacity of stem/progenitor cells to self-organise into microtissues or organoids, which can be used as the building blocks of larger grafts. In this study, adult human bone marrow-derived mesenchymal stem/stromal cells (hMSCs) were used to engineer phenotypically distinct hyaline cartilage microtissues for the modular assembly of zonally defined grafts. Altered oxygen (O_2) levels, within the physiological range, were first explored to modulate the microtissue phenotype. Melt electrowritten (MEW) meshes were then used to guide the fusion of such microtissues into scaled-up grafts. Priming hMSC-derived microtissues at oxygen levels representative of different regions of the native tissue supported the development of distinct cartilaginous phenotypes. In addition, short-term exposure to 2% O_2 significantly enhanced the deposition of glycosaminoglycans compared to exposure to 5% O_2. Combining such microtissues with a supporting MEW mesh enabled the development of a larger graft with controlled geometry. In conclusion, this study highlights the potential of hMSC-derived cartilage microtissues, primed under altered oxygen environments, as building blocks for the biofabrication of articular cartilage grafts when combined with supporting MEW meshes.

Keywords

tissue engineering, mesenchymal stem/stromal cells, microtissues, hyaline articular cartilage, oxygen, glycosaminoglycans, modular assembly, MEW mesh

Graphical Abstract

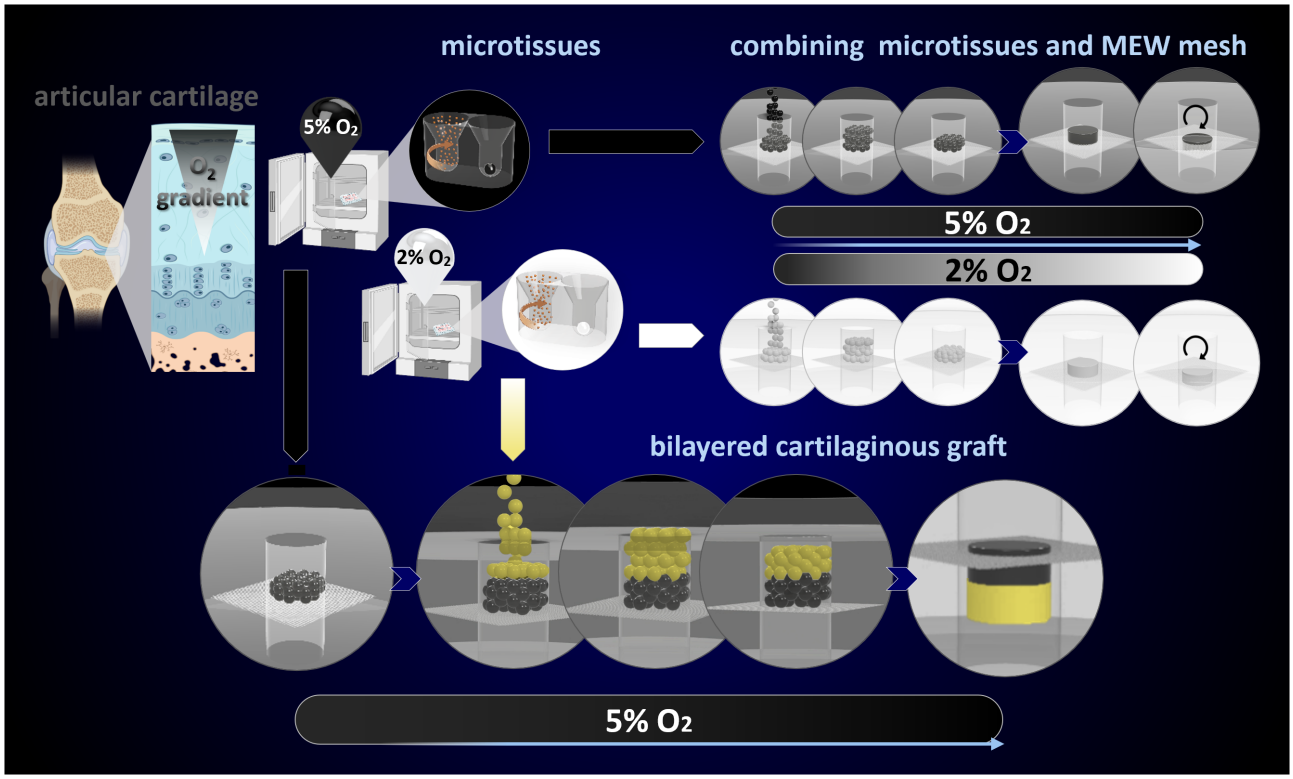

Highlights

- Altered O_2 levels support differential chondrogenesis in hMSC-derived microtissues
- Short exposure to low O_2 levels enhances GAG deposition in cartilage microtissues
- A new modular assembly method using MEW meshes supports scaled-up graft development

1. Introduction

Articular cartilage (AC) exhibits a well-defined spatial composition and organisation, characterised by zonal gradients in cellular shape and extracellular matrix (ECM) composition. Notably, concentrations of glycosaminoglycans (GAGs) increase progressively from the superficial zone to the deep zone, where they reach their highest levels, in parallel with spatial variations of collagen content [1]. AC has a poor self-healing ability [2] and untreated damaged tissue typically degenerates, increasing the risk of developing post-traumatic osteoarthritis (OA) [3]. Shortcomings associated with current treatments for focal cartilage damage have motivated increased interest in innovative tissue engineering (TE) strategies for synovial joint regeneration [4]. However, the engineering of regenerative grafts that mimic the intricate zonal nature of AC remains a challenge [5].

Developmentally inspired tissue engineering strategies can potentially overcome limitations associated with current approaches, leading to the development of more biomimetic grafts by mimicking key steps of normal tissue development. One such approach leverages the capacity of stem/progenitor cells to self-organise into microtissues or organoids [6], which can then be used as biological building blocks to fabricate larger grafts. For example, seeding mesenchymal stem/stromal cells (MSCs) into nonadhesive micro-moulds has been shown to promote cell-cell interactions and the development of hyaline cartilage microtissues [7-9]. Self-assembly of such spheroids or microtissues into larger tissues presents several challenges, including maintenance of tissue geometry, handleability, and ensuring sufficient nutrient and oxygen (O_2) transport within the scaled-up graft [10, 11]. Furthermore, it remains unclear how the zonal complexity present in tissues such as AC can be recapitulated using such tissue engineering strategies.

To increase their overall structural stability, cellular spheroids or microtissues are often combined with macroporous scaffolds to generate more mechanically robust constructs [12]. One concern with this approach is that large volumes of scaffold material might negatively impact microtissue (re)modelling and/or promote a foreign body response once implanted into the body. For example, the fibres of scaffolds printed by fused deposition modelling (FDM) are usually thick (>100 μm) and could account for more than 30% of the construct [13]. Similar to FDM, melt electrowriting extrudes molten polymers through a nozzle but in the presence of a high electric field, resulting in the production of extremely thin fibres (down to micron size [14]), and the generation of highly porous (typically 90–98%) scaffolds with lower polymer contents [15-17]. The geometry of such melt electrowritten (MEW) scaffolds can also be precisely modulated to help direct MSC differentiation [14] and guide collagen fibre organisation [18, 19]. Cellular spheroids generated within MEW scaffolds using inkjet bioprinting were previously shown to generate a large sheet-like tissue with a stratified collagen orientation, demonstrating that such hybrid engineered constructs can be used to generate tissues with native-like organisation [20]. Different preformed microtissues have also been combined with MEW sheets to generate implants targeting adipose regeneration [16, 21] and bone repair *in vivo* [13]. These studies support the use of MEW scaffolds to support the bio fabrication of microtissue-based grafts. Successfully engineering complex tissues such as AC or the osteochondral unit using such approaches will also require the engineering of phenotypically distinct microtissues representative of the different regions of the target tissue and their subsequent assembly into spatially organised grafts.

Due to its avascular nature, oxygen tension varies through the depth of AC [22], with models predicting a variation from 5% to 1% O_2 [23] and *in vivo* measurements further confirming that levels range from 5 to 7% at the surface to 0.5–1% in the deeper regions of the tissue [24-26]. Local oxygen levels are key regulatory cues in tissue development, homeostasis and repair [27]. During limb development, hypoxia plays a key role in normal cartilage formation [28]. Cells typically used in the regeneration of AC (chondrocytes [29], MSCs [30-35], articular cartilage progenitors (ACPs) [36]) have been shown to be highly sensitive to low oxygen environments, with hypoxic conditions typically promoting a chondrogenic phenotype and enhanced cartilage-specific ECM production [37, 38]. However, in such studies, low oxygen conditions (2–5% O_2) are typically compared to non-physiological normoxic levels (20–21% O_2). Therefore, it remains unclear how cells used for the engineering of zonally defined AC grafts might respond to the variations in oxygen tension typically observed in the native tissue. While numerous studies have explored the influence of 5% O_2 on chondrogenesis of MSCs, mimicking the levels found at the surface of AC, relatively fewer studies have examined the role of lower oxygen levels (2% O_2 and below) representative of the deeper zones of AC [36, 39], with concerns that very low oxygen levels can be detrimental to the production of collagen [40]. This motivates further studies comparing the influence of altered oxygen levels representative of the different zones of AC on chondrogenesis of MSCs. In the context of engineering hyaline cartilage, mimicking the oxygen gradient that contributes to normal AC development and homeostasis may contribute to the development of phenotypically distinct microtissues representative of the different regions of the native tissue.

The overall aim of the study was to engineer zonal AC grafts by integrating phenotypically distinct cartilage microtissues into supporting MEW structures. To this end, we first sought to generate cartilage microtissues with distinct zonal phenotypes using human MSCs (hMSCs) differentiated under oxygen levels representative of the surface (5%) and deeper (2%) regions of native AC. To explore the influence of short-term low oxygen priming on longer-term phenotype, we also explored the influence of maintaining hMSC-derived microtissues for 7 days at 2% O_2 before increasing it to 5% O_2 for the remainder of the culture period. Such oxygen-primed cartilaginous microtissues were then integrated into a MEW mesh with custom pore sizes which functioned to collect and nest individual microtissues in a predefined manner. The MEW mesh was designed with minimal material volume so as to not impede microtissue fusion, whilst also guiding the (re)modelling of microtissues into a structurally organised graft. We also explored how the orientation of the engineered grafts will influence their development by either hanging the microtissues from the MEW mesh or allowing the tissue to grow upwards from the base of the MEW mesh. Finally, a layered construct was created using microtissues primed under altered oxygen conditions in an attempt to recapitulate the compositional gradient observed through the depth of native AC.

2. Materials and Methods

2.1. Tissue Isolation and Processing

Human cartilage tissue was collected with informed written consent with ethical approval from surgical waste of patients undergoing partial or total knee replacement at National Orthopaedic Hospital Cappagh (NOHC), Dublin, Ireland (Capp/2019/ETH/SH-CEO-234). Chondral plugs were cut from healthy-looking regions using biopsy punches until the subchondral bone. Tissues were washed with phosphate buffer saline (PBS) and frozen until processing. The plugs were cut into two regions: the surface region corresponding to approximately the top one third and the deep region corresponding to approximately the bottom two thirds (confirmed by weight). Tissues were then prepared for biochemical analysis.

2.2. Human MSC – Chondrogenic Differentiation

2.2.1. Expansion of hMSCs

Human MSCs were isolated from the three different human bone marrow donors (Lonza) as previously described prior to expansion [41]. Alternatively, hMSCs were directly expanded from a commercially available source (RoosterBio) for single layer experiments. Cells were expanded from an initial cell density of 3,000 cells/cm2 at 5% O_2 and 5% CO_2 at 37 °C in humidified atmosphere until subconfluency. Expansion media (XPAN) contained high glucose Dulbecco's Modified Eagle Medium GlutaMAX, 10% v/v foetal bovine serum, 100 U/mL penicillin, 100 μg/mL streptomycin (all Gibco) and 5 ng/mL fibroblast growth factor 2 (Prospect Bio). XPAN was changed twice a week, and cells were expanded until passage 3 prior to microtissue formation.

2.2.2. Microtissue Formation and Chondrogenic Differentiation

Agarose (4% w/v in PBS) microwells (1.5 mm depth × 1 mm diameter) were moulded under sterile conditions following the protocol of Nulty et al. [42]. Soaking media (XPAN for 24 h) was removed and a 1,604,000 cells/3 mL of XPAN suspension was pipetted onto the microwell array, settled for 15 min, spun at 800 ×g for 5 min, resulting in individual microtissues containing 4,000 cells each. After 24 h, XPAN was replaced by chondrogenic differentiation media (CDM) was added. CDM contained high glucose Dulbecco's Modified Eagle Medium GlutaMAX, 100 U/mL penicillin, 100 μg/mL streptomycin (both Gibco), 1.5 mg/mL bovine serum albumin, 40 μg/mL L-proline, 100 μg/mL sodium pyruvate, 1 × insulin-transferrin-selenium, 100 nM dexamethasone, 50 μg/mL L-ascorbic acid-2-phosphate, 4.7 μg/mL linoleic acid (all from Sigma) and 10 ng/mL human transforming growth factor (TGF)-β3 (Peprotech). CDM was replaced by freshly prepared media every 2–3 days. Microtissues were maintained at desired oxygen conditions (2% or 5% O_2) for 2 days, 7 days or 21 days, except for the priming group (2–5%) where microtissues were maintained at 2% O_2 for 7 days and then placed at 5% O_2 for 14 days (21 days of total study time). Other variables were maintained constant (5% CO_2, 37 °C, humidified atmosphere). At the end of the culture period, microtissues were dislodged from their microwell. The number of harvested microtissues was recorded and the diameter of microtissues (averaged from three measurements) was measured using the Fiji length measurement tool on brightfield microscopy images.

2.2.3. Combining Microtissues and MEW Meshes

2.2.3.1.Fabrication of a MEW Mesh-Bottomed Well

Polydimethylsiloxane (PDMS) insert — PDMS was prepared according to the manufacturer's instruction (SYLGARDTM 184 Silicone Elastomer Kit, Dow). Inserts with the following dimensions were punched using biopsy punches: 5 mm outer diameter, 3 mm inner diameter and 5 mm in height. Inserts were washed in PBS, in ethanol for 30 min and finally were rinsed in PBS before use.

MEW mesh — MEW meshes were printed using a custom-built MEW printer [43]. The Capa 6500D polycaprolactone (50,000 MW, PCL, Perstorp) was melted at 80 °C and extruded at 5 mm from the collector through a 23G needle heated up to 85 °C under 0.6 bar. An initial voltage of 6 kV was applied with an increase of 0.025 kV per layer. Printing pore dimensions were: 200 μm × 200 μm, 210 μm × 210 μm, 220 μm × 220 μm, 230 μm × 230 μm, 240 μm × 240 μm or 250 μm × 250 μm. The printed pore dimensions were measured using the Fiji length measurement tool on brightfield microscopy images. Three hundred measurements were taken from three different regions of printed meshes. Fibre diameter was 10 μm. Pore wall was only six fibres in height, corresponding to theoretical value between ~60 μm and ~120 μm, to minimise the presence of biomaterials without compromising the pore wall stability. A "fitting" pore size was chosen using the following equation, where D is the size (diameter) of the microtissue (μm), P is the pore size of the mesh (μm) and H is the height position of the mesh (% of the microtissue size):

$$H = (((D/2) - 0.5 \times (D^2 - P^2)^{1/2})/D) \times 100$$

Fig. S1 shows the relative variations of H to D and P, and was used to select the pore size depending on the microtissue size. Then, a 1 cm × 1 cm mesh was cut out and treated with 5 M sodium hydroxide for 30 min, washed in PBS and in ethanol for 30 min. The mesh was air-dried overnight and ultraviolet (UV) sterilised for 30 min. Finally, the mesh was coated with 10 μg/mL of fibronectin (Merck) in PBS for 24 h.

Fabrication of a MEW mesh-bottomed well — MEW mesh-bottomed wells were fabricated using 6-well plates. A fibronectin-coated MEW mesh was maintained between PDMS inserts. Sterile 2% w/v agarose in PBS was molten at 60 °C, to avoid melting the PCL fibres, and poured around the inserts. After gelling of the agarose, the inserts were pulled out, creating a 5 mm × 5 mm well which the bottom part consisted of a MEW mesh. Finally, 6 mL of XPAN was added for 24 h prior to microtissue seeding.

2.2.3.2.Assembly of Scaled-up Grafts

2.2.3.2.1.Single-Layer Assembly

Microtissues were primed for 7 days at 2% or 5% O_2. The priming period was selected based on previous results to maximise the effect of oxygen on the resulting cartilaginous phenotype without compromising microtissue fusion [44]. A theoretical number of 1,200 microtissues were suspended in 100–200 μL of CDM and seeded onto the MEW mesh-bottomed well. Each well was topped up with 6 mL of freshly prepared CDM and cultures were returned to their initial oxygen environment. After 2 days of initial fusion, the effect of orientation on the organisation of the collagen network was explored by turning constructs upside down so the fusing grafts were hanging from the MEW mesh (hanging group) while other constructs were kept as control (sitting group – see Table 1).

After 21 days of culture, the scaled-up tissues were cut in half: one half for biochemical assays and one half for histological and immunofluorescence staining.

Table 1 Experimental outline of single-layer assembly experiments.

Groups	Single Microtissues—O_2 (%)	Fused Microtissues	
		O_2 (%)	orientation
5H	5	5	hanging
5S	5	5	sitting
2H	2	2	hanging
2S	2	2	sitting

2.2.3.2.2.Bilayered Hybrid Tissue Assembly

Microtissues, used to fabricate the first/top layer of the graft, were cultured for 7 days at 5% O_2. Microtissues, used to fabricate the second/bottom layer of the graft, were cultured for 7 days at 2% O_2. As previously described, a first layer of 7-day-old microtissues primed at 5% O_2 was added onto the MEW mesh and topped with CDM for 2 days until the second layer was added. To achieve this, 7-day-old microtissues primed at 2% (theoretical number of 1,200) were suspended in 50–100 μL of CDM and added over the first layer. Fresh CDM was added and the bilayered graft was returned at 5% O_2 for the rest of the culture period (42 days total). Grafts were left untouched for 2 days to facilitate the fusion of the second layer and the inter-layer integration. Then, the grafts were either hung upside down or left sitting. Timeline is summarised in Table 2.

Table 2 Experimental outline of the modular assembly of bilayered grafts.

Day	O_2 (%)	Step	FD[1]
0	5	priming single microtissues	-
2	2	priming single microtissues	-
7	5	seeding of 5% O_2 primed microtissues on MEW mesh (1st layer)	0
9	5	seeding of 2% O_2 primed microtissues (2nd layer)	2
11	5	hanging of bilayered engineered grafts	4
42	5	histological and immunofluorescence analysis	35

[1] FD: fusion day.

2.2.4.Microtissue Fusion in a Nonadherent Agarose Well

To confirm the guiding effect of the MEW mesh on the collagen network, a 4 mm × 5 mm nonadherent well was fabricated using 2% w/v agarose in PBS and a PDMS insert. A theoretical number of 1,200 microtissues primed for 7 days at 5% O_2 were seeded in the

nonadherent well. CDM was changed three times per week and tissues were maintained at 5% O_2.

2.3. Biochemistry Quantification of Extracellular Matrix Key Components

At determined timepoints, samples were digested in 3.88 U/mL papain enzyme in papain buffer extract (PBE – containing 100 mM sodium phosphate buffer and 5 mM ethylenediaminetetraacetic acid disodium salt solution) containing 10 mM L-cysteine (pH 6.5) overnight at 60 °C. Total deoxyribonucleic acid (DNA) content was quantified by bisBenzimide Hoechst fluorescent assay as described by the manufacturer. Total GAGs were quantified using 0.002% w/v 1,9-dimethyl-methylene blue dye solution, 0.25% w/v sodium chloride and 0.3% w/v glycine (pH 1.5). Diluted series of shark chondroitin sulphate in PBE were used as standards. Total collagen content was calculated from the measurement of the hydroxyproline content (hydroxyproline-to-collagen ratio of 1:7.69) as previously described [45, 46]. After hydrolysation of proline residues using 12 M hydrochloric acid overnight at 110 °C, solid material was dried out and resuspended in ultrapure deionised water. Then, oxidising 2.82% w/v chloramine T in citrate buffer (pH 6.1) was added for 20 min at RT in the dark, followed by addition of 50% w/v 4-(dimethylamino)benzaldehyde for 20 min at 60 °C. Serial dilutions of trans-4-hydroxy-L-proline (Fluka) in PBE were used as standards. All reagents were from Merck if not mentioned otherwise. Measurements of standards and samples were carried out using the Synergy HT Multi-Mode Microplate Reader (BioTek Instruments, Inc): DNA – fluorescence at 360 nm (ex)/460 nm (em), GAG – absorbance (ε extinction coefficient) at 530 nm and 590 nm (ε 530/ε 590) [47, 48], collagen – absorbance at 570 nm.

2.4. Staining Procedure and Quantification

Histology staining — At determined timepoints, samples were fixed using 4% w/v paraformaldehyde solution overnight at 4 °C. Following embedding in 2% w/v agarose, samples were dehydrated in a graded series of ethanol solutions (Leica TP 1020). All samples were embedded in paraffin wax and sectioned into 7 μm thick sections using a rotary microtome (Leica RM2235). Sections were stained with Haematoxylin and Eosin, 0.1% w/v Picrosirius Red and 1% w/v Alizarin Red (pH 4.1). GAGs were either stained with 1% w/v Alcian Blue 8GX in 0.1 M hydrochloric acid (pH 1) (0.1% w/v Nuclear Fast Red cell counterstain) or with 0.2% w/v Safranin O, 0.04% w/v aqueous Fast Green (counterstain) and Weigert's Iron Haematoxylin (to counterstain cells). All reagents were from Merck. Stained sections were imaged using a slide scanner (Aperio ScanScope CS).

Immunofluorescent staining — Tissue sections were rehydrated in graded series prior to antigen retrieval. Tissue sections and meshes coated with 10 μg/mL fibronectin were incubated in serum containing solutions for 1 h at room temperature (RT) in a humidity chamber (HC) to block unspecific antigen sites. Primary antibodies and fluorescently labelled secondary antibodies were diluted in blocking buffer and incubated overnight at 4 °C in a HC and 1 h in the dark at RT in a HC, respectively. Prior to imaging, mesh slides were mounted in ProlongTM Gold Antifade Mountant (Invitrogen) and tissues sections were mounted in Fluoroshield with 4',6-diamidino-2-phenylindole (DAPI). Staining was visualised using a scanning confocal microscope (LeicaTCS SP8) and images were taken as z-stacks of 10 images. Images were processed using Leica Application Suite X (version 3.7.4.23463). Exposure was set using the negative and positive controls, and same settings were used for all samples. More details about the staining procedure are found in Table S1.

Quantification — Histology (fluorescence) stain intensity was quantified on multicoloured (8-bit) brightfield images using the Fiji Colour Histogram tool. The mean values of red, green, and blue colours (the mean grey value (MGV)) of a microtissue area, RGBμT (MGVμT), were averaged (was measured). Three background areas surrounding each microtissue were selected and the averaged RGBbackground (MGVbackground) was calculated. The staining intensity was graphed using the following formula: 1 - (RGBμT / RGBbackground) or (MGVμT - MGVbackground), so the 0 value corresponds to RGBμT (MGVμT) equals to RGBbackground (MGVbackground).

2.5. Polarised Light Microscopy

Polarised light microscopy (PLM) was used to visualise collagen fibres in tissue sections stained with Picrosirius Red. Two sections, one from the periphery and one from the centre of the construct, were analysed per replicate. Two replicates were analysed per experimental group. Orientation analysis was performed using Fiji. Two PLM images (PLM filter orientated at 0° and 45°) per section were collected and merged using a maximum intensity projection and were then converted into 8-bit images. Colour maps were generated using the OrientationJ Analysis plugin (color gradient generated using the cubic spline method (hue: fiber orientation (red/pink = ± 90°, cyan = 0°); saturation: fiber coherency; unit = 2 pixels)). Resulting merged images and colour maps are presented in Fig. S2. The distribution of fibre orientations was measured using the Directionality feature (Fourier component method; bin = 5°). Histograms were generated for 3 distinct regions of the tissue [49]: surface and deep, corresponding to the regions of the engineered graft containing the MEW mesh in the hanging and sitting groups, respectively, and middle. Spatial organisation of collagen in knee articular cartilage shows that fibres are horizontal at the surface and vertical in the deep region. Hence, to assess the local organisation of the engineered graft, like the native tissue, the aforementioned divisions were used. These regions are represented in Fig. S2. The dominant fibre orientation and the fibre coherency were measured with the OrientationJ Dominant Direction plugin. To assess the effect of the MEW mesh on the collagen fibres dominant orientation and coherency, regions of interest from the region containing the MEW mesh (superficial) and from regions not containing the MEW mesh (deep) were selected and analysed.

2.6. Statistical Analysis

The GraphPad Prism 10 software (GraphPad Software, CA, United States) was used to analyse statistical differences. Analysis of Gaussian distribution and statistical tests are detailed on a case-by-case basis in each figure caption.

3. Results

3.1. Altered Oxygen Levels Yield Chondrogenic Microtissues with Distinct Phenotypes

The phenotype of hMSC-derived microtissues, engineered under altered oxygen tensions (2% or 5% O_2), was first assessed using a range of biochemical, histological and immunofluorescent assays of chondrogenic characteristics. For both oxygen levels, DNA levels after 7 days and 21 days of chondrogenic differentiation were significantly lower than that observed on day 2 (Fig. 1(A)). GAGs/DNA was significantly higher at 2% O_2 than at 5% O_2, reaching 11.3 $\mu g/\mu g$ ± 2.2 $\mu g/\mu g$ on day 21 at 2% O_2 (Fig. 1(B)). Total collagen synthesis was not significantly affected by oxygen conditions after 21 days of culture (Fig. 1(C)).

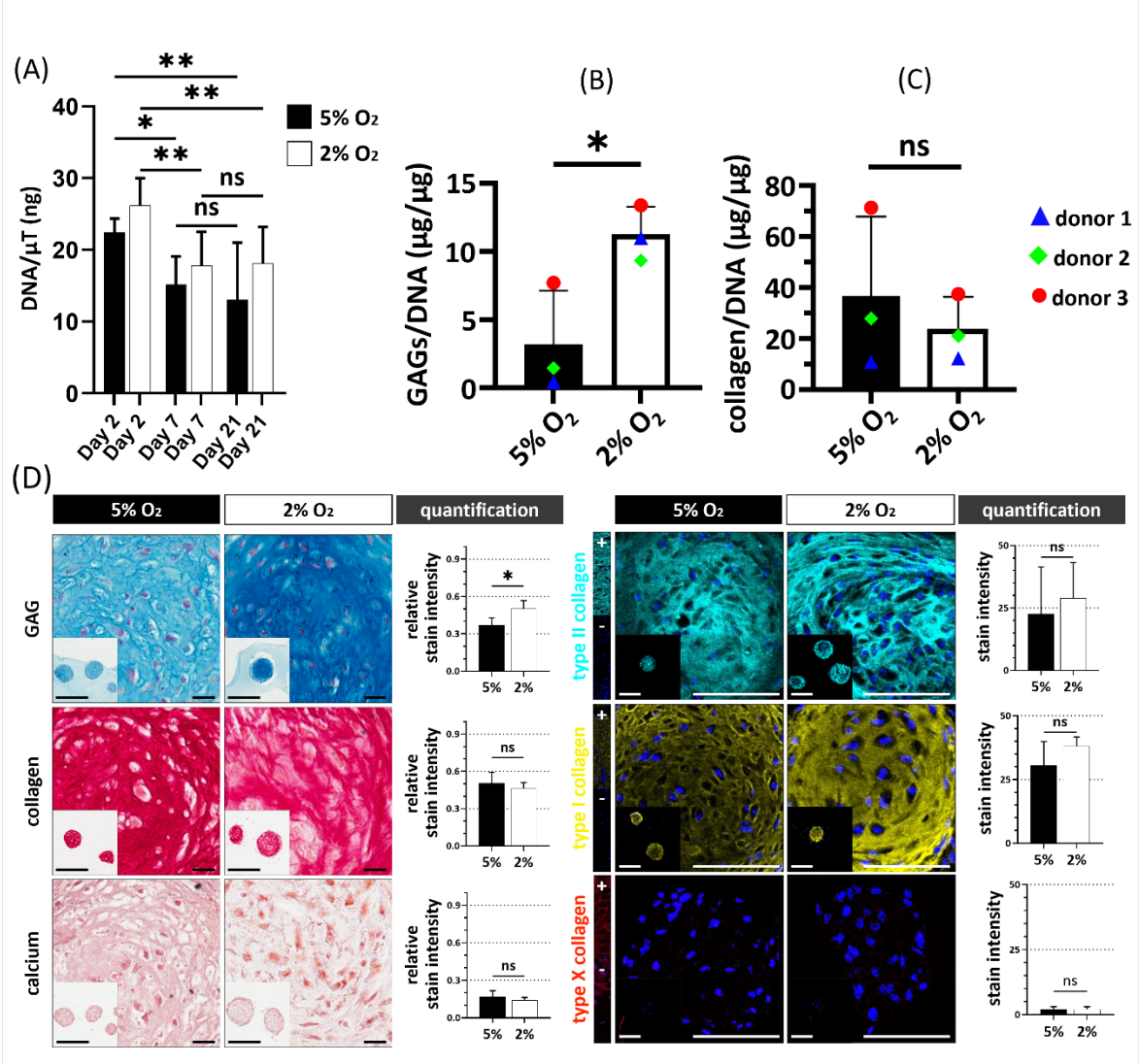

Fig. 1 Characterisation of human mesenchymal stem/stromal cell (hMSC)-derived chondrogenic microtissues differentiated under altered oxygen (O_2) environments. Biochemical quantification of (A) deoxyribonucleic acid (DNA) per microtissue under 2% or 5% O_2 at day 2, 7 and 21. Biochemical quantification of (B) glycosaminoglycans (GAGs) normalised by DNA, and (C) collagen normalised by DNA of microtissues differentiated under 2% or 5% O_2 at day 21. All data is represented as mean ± standard deviation and individual data points ((B)&(C)). Statistical differences were determined by one-way ANOVA test with Holm-Šidák's multiple comparison test ((A)) and by paired t-test ((B)&(C)). Normality was determined using D'Agostino & Pearson's test (A) and Shapiro-Wilk's test ((B)&(C)). N ≥ 6 ((A)) and N = 3

((B)&(C)). ns denotes not significant, * denotes p <0.05, ** denotes p <0.01, *** denotes p <0.001, **** denotes p <0.0001. (D) Stain panel of microtissue-synthesised extracellular matrix (nuclei are shown in dark blue in immunofluorescence images) and stain intensity quantification at day 21. Scale bar = 100 μm / 400 μm (inserts). All data is represented as mean ± standard deviation. Statistical differences were determined by Student t-test for histology stains (N = 4, normal distribution according to Shapiro-Wilk's test) and nonparametric Mann-Whitney test for immunofluorescence stains (N ≥3). ns denotes not significant, *p <0.05. +: positive control; -: negative control. (For interpretation of the references to color in this figure legend, the reader is referred to the web version of this article.)

After 21 days of culture microtissues stained positive for GAGs and collagen but were negative for calcium accumulation (Fig. 1(D)). GAG staining was generally homogeneous throughout the microtissues, but more intense in the 2% O_2 group than the 5% O_2. A semi-quantitative evaluation of staining intensity confirmed these observations. Collagen staining was generally homogeneous at 5% O_2, but at 2% O_2 was generally stronger at the periphery of the microtissues and less intense in the centre. Cells in both the centre and periphery appeared chondrocyte-like, with a round shape and the presence of a lacuna. Under both oxygen environments, microtissues stained positive for type II collagen, with no statistical differences in staining intensity observed. Microtissues also stained positive for type I collagen accumulation, but negative for type X collagen staining for both oxygen groups. Together these results indicated that the composition of hMSC-derived microtissues is altered by the oxygen environment during chondrogenic differentiation and that phenotypically distinct cartilage microtissues can potentially be engineered by careful control of local oxygen levels.

3.2. Microtissues Primed for One Week at 2% Oxygen Secrete Higher Levels of Glycosaminoglycans in Long-term Culture

Having found that microtissue phenotype is altered in low oxygen conditions (as evident by altered GAG production), the effect of short-term low oxygen priming on longer term tissue development was next assessed. Microtissues were either differentiated at 5% or 2% O_2 for 21 days, or first primed at 2% O_2 for 7 days and then moved to 5% O_2 for 14 days (a total culture period of 21 days) to assess if differences in GAG content associated with a relatively short-term exposure to 2% O_2 will persist when such microtissues are then exposed to higher oxygen levels (5% O_2) (Fig. 2(A)). Oxygen tension had no effect on DNA levels (Fig. 2(B)), including when microtissues were exposed to altering oxygen conditions (2–5% O_2). GAG levels were significantly higher in microtissues exposed to altering oxygen conditions (2–5% O_2) than those continuously exposed to 5% or 2% O_2 (Fig. 2(C)). These results suggest that the enhanced GAG production in low oxygen-primed microtissues will persist when later maintained in higher oxygen conditions.

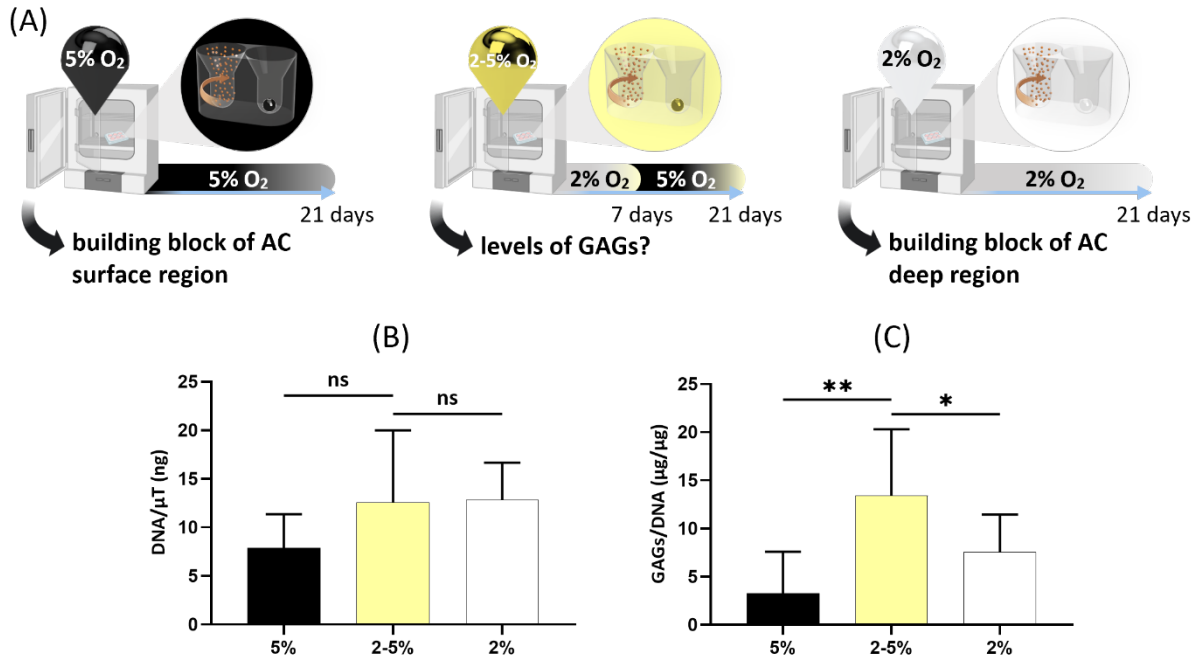

Fig. 2 Comparison of the GAG content of chondrogenic microtissues differentiated under three different oxygen conditions. (A) hMSC-derived microtissues were cultured at 5% or 2% O_2 for 21, or for 7 days at 2% O_2 followed by 14 days at 5% O_2 (2–5%P). AC: articular cartilage. (B) DNA per microtissue and (C) GAGs normalised by DNA biochemical quantification at day 21. All data is represented as mean ± standard deviation. Statistical differences were analysed by one-way ANOVA test with Holm-Šídák's multiple comparison test as all groups followed a normal distribution according to D'Agostino and Pearson's test. N = 9. ns: not significant, *p <0.05, **p <0.01.

3.3. Assembly of Cartilage Microtissues onto a Supporting MEW Mesh

MEW scaffolds have previously been used to guide collagen orientation within engineered tissues [18]. To guide the orientation of collagen fibres deposited by hMSC-derived microtissues, a novel modular assembly strategy was developed where a MEW mesh maintained inside an agarose well was leveraged to structurally support the fusion and (re)modelling of the microtissues. To enhance cell adhesion and promote maintenance of tissue geometry [50], the MEW meshes were coated with fibronectin prior to their insertion into the agarose wells (Fig. 3(B)). The MEW meshes (1 cm × 1 cm) were placed between two PDMS cylindrical (5 mm × 3 mm × 5 mm) inserts (Fig. 3(A) ①-④). The inserts were maintained in place with a custom-made 3D printed handle cover (not represented). Molten 2% w/v agarose was added around the inserts to entrap the MEW mesh (Fig. 3(A) ⑤). After gelation, the top insert could easily be removed using tweezers (Fig. 3(A) ⑥). The system was then flipped upside down to remove the other insert (Fig. 3(A) ⑦-⑧). As seen in the top and side views, the positive inserts left behind an empty cylindrical well, with the MEW mesh remaining in its centre creating a MEW mesh-bottomed well (Fig. 3(D)). The system was soaked in XPAN prior to microtissue seeding (Fig. 3(A) ⑨). Meshes with a range of different theoretical pore dimensions were printed (200 µm × 200 µm, 210 µm × 210 µm, 220 µm × 220 µm, 230 µm × 230 µm, 240 µm × 240 µm, 250 µm × 250 µm). Measurements of the pore size showed that pore size fidelity increased with printed pore size (Fig. 3(C)).

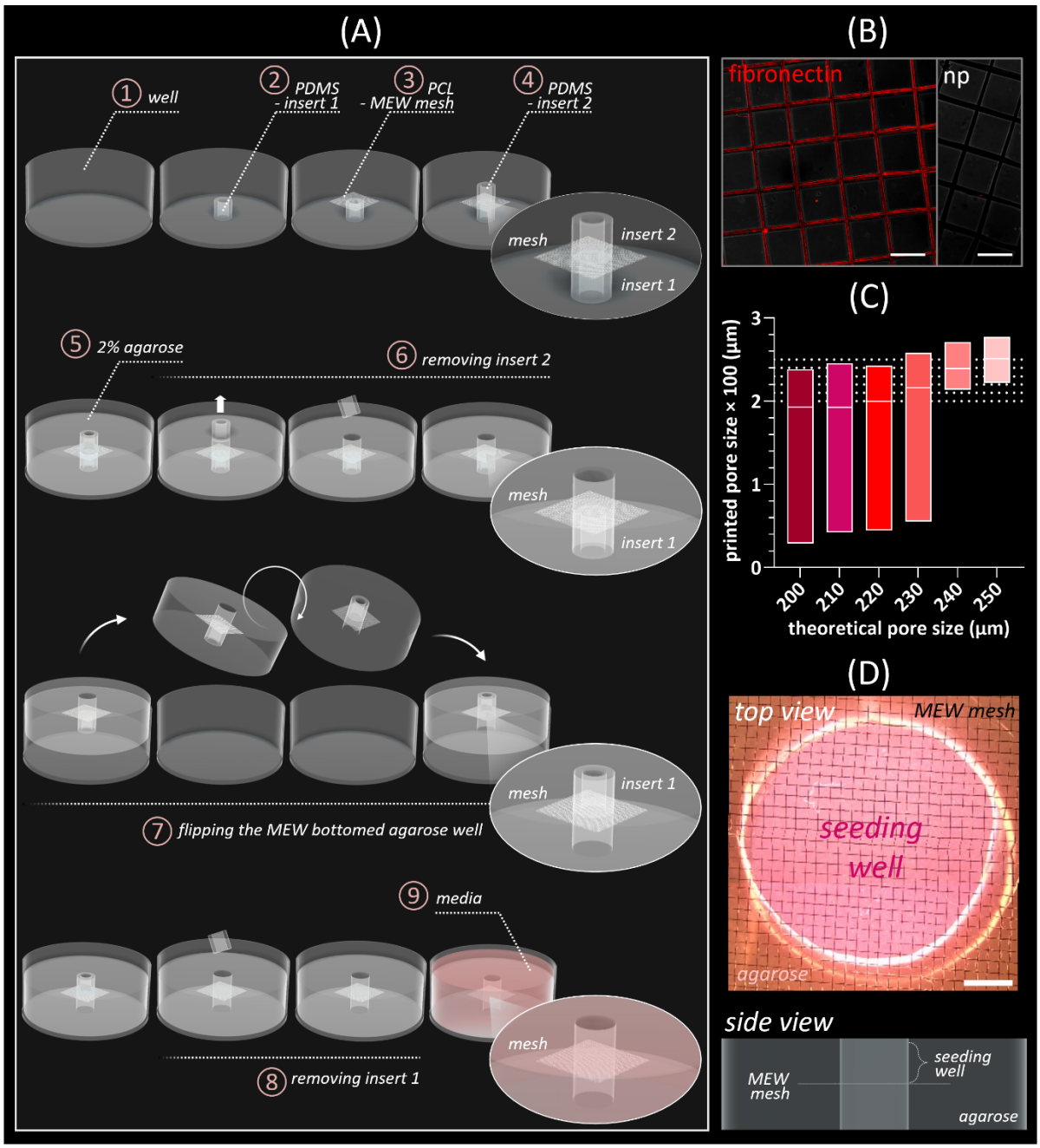

Fig. 3 Fabrication of a novel melt electrowritten (MEW) mesh-bottomed well. (A) Schematic of the fabrication steps of the MEW mesh-bottomed well. (B) Confocal images of the fibronectin coating of the MEW mesh (side view). Scale bar = 200 μm. np: no primary (negative control). (C) Distribution of the measured MEW pore size for each theoretical printing dimensions (box-like) showed as dotted lines. Data is represented as min to max floating bars with line indicating median. (D) Schematic (side view) and picture (top view) of the MEW mesh-bottomed agarose seeding well. Scale bar = 1 mm. PDMS: polydimethylsiloxane; PCL: polycaprolactone.

The MEW mesh was designed to support a single individual microtissue inside each of its pores. The goal was to print a mesh with a pore size that allowed the collection of microtissues without having them sitting too high, which could interfere with the integration of microtissues with the MEW mesh, while simultaneously preventing them from passing through the bottom of the MEW pores (Fig. 4(A)). This configuration should promote the fusion and direct the growth of microtissues into a millimetre scale construct. As seen in brightfield images, microtissues were successfully collected (theoretical number of 1,200), resulting in a theoretical layer depth of 2–3 microtissues being deposited onto the surface of the MEW mesh (Fig. 4(B)). After the initial fusion (Fig. 4(C)), no further contraction of the

newly formed tissue (average of 29% ± 15% of contraction across all experimental groups) was observed during the remainder of the culture period (as had been observed in the absence of the guiding mesh; see Fig. S3(A)). The resulting constructs were approximately 2.5 mm in diameter and 1.5 mm in thickness (Fig. 4(D)).

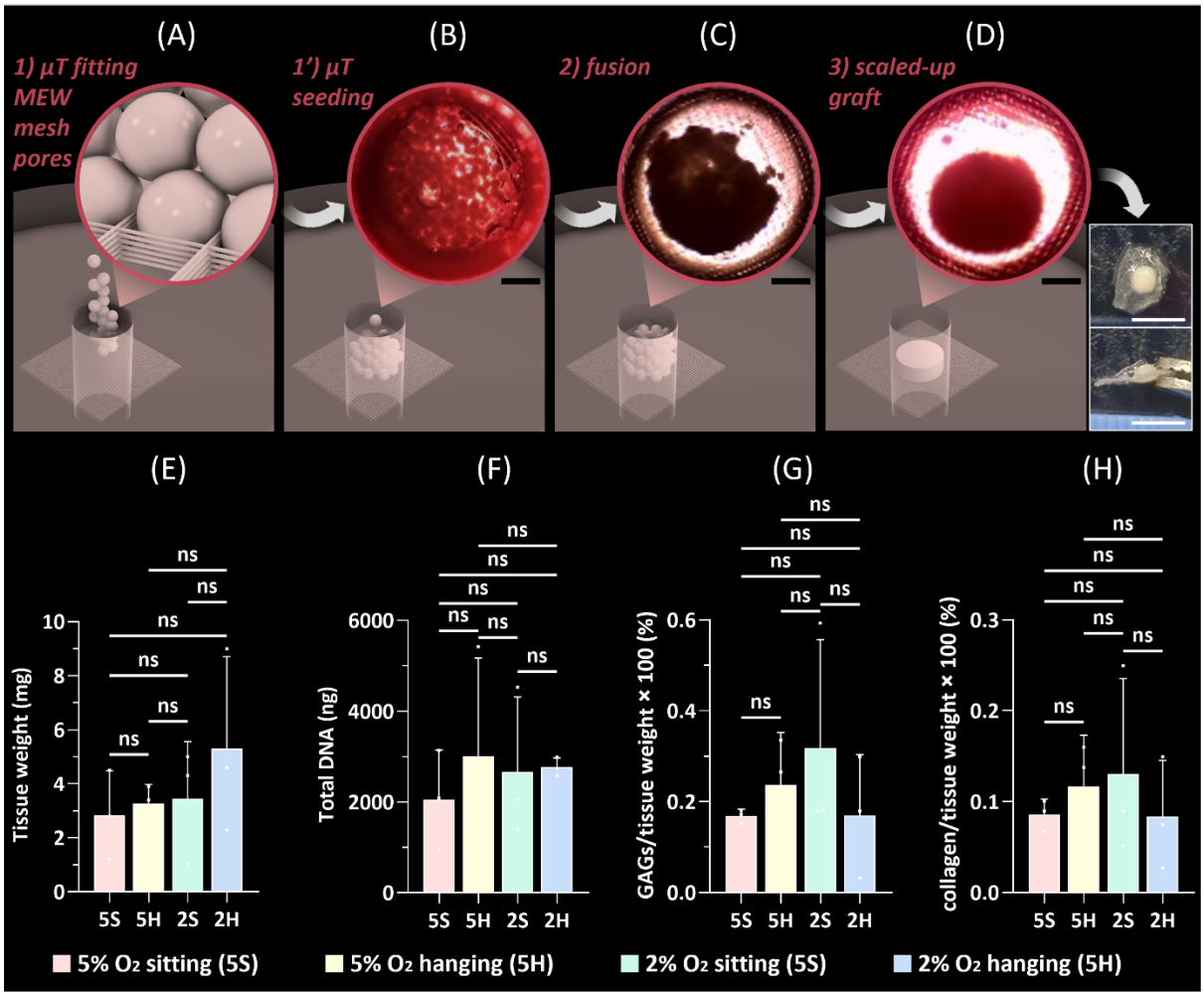

Fig. 4 Fabrication method of scaled-up grafts. Schematic and pictures of (A) microtissue seeding onto a MEW mesh-bottomed agarose seeding well and (B)&(C)&(D) subsequent self-organisation. Scale bar = 1 mm (brightfield) / 5 mm (photographs). Biochemical quantification of (E) graft wet weight, (F) total DNA, and (G) GAGs and (H) collagen normalised by weight after 21 days of culture at 5% O_2 and 2% O_2, and in sitting and hanging orientations. All data is represented as individual data points and mean ± standard deviation. Statistical differences were analysed by one-way ANOVA test with Holm-Šídák's multiple comparison test. ns: not significant. μT: microtissue.

The new fabrication platform was tested by seeding microtissues in the MEW mesh-bottomed well and maintaining the construct in TGF-β3 for 21 days at 5% O_2 or 2% O_2 (Fig. S4). To investigate their fusion capacity, 7-day-old microtissues generated at 2% O_2 and 5% O_2 were seeded onto the MEW mesh. In addition, the role of graft orientation on microtissue fusion and tissue development within this system was also explored. To this end, in one group (called sitting) microtissues stayed onto the MEW mesh, while in a separate group (called hanging) the construct was flipped upside down shortly after microtissue seeding to investigate the effect of hanging the microtissues from the MEW mesh on the resulting collagen network organisation. Before their seeding onto the MEW mesh, the diameter of the microtissues after 7 days of chondrogenic differentiation was found to be 241 μm ± 48 μm for the 5% O_2 group and 236 μm ± 55 μm for the 2% O_2 group. Based on this, a MEW pore size of 230 μm × 230 μm, where approximately 40% of

the microtissue is sitting within the MEW mesh, was selected to support the microtissues (Fig. S1). Hanging tissues from the MEW mesh did not negatively affect the tissue weight (Fig. 4(E)) and the levels of DNA (Fig. 4(F)) compared to the sitting group. Additionally, total GAGs and collagen production were not statistically different across the groups (Fig. 4(G)&(H)).

In histological staining, the attachment points of the neo-tissue to the MEW mesh were visible at the edge of the constructs (at the bottom of the tissues for the sitting groups and at the top of the tissues for the hanging groups (Fig. 5(A)). Anchoring the fusing microtissues to the MEW mesh was sufficient to generate a geometrically uniform tissue. All engineered tissues stained positive for GAGs and collagen. Calcium deposition was observed in some regions of the tissues. Immunofluorescent staining for type II collagen was observed primarily at the periphery of the construct, with the highest levels of staining observed in the 2% O_2 hanging group (Fig. 5(B)). Some donor-to-donor variation was observed in this study. For two of the donors, enhanced type II collagen deposition was observed in the 2% O_2 hanging group, while for a third donor the highest level of type II collagen deposition was observed in the 5% O_2 hanging group (Fig. S5). No statistical differences in type II collagen stain intensity were observed between experimental groups (Fig. S6). All groups stained positive for type I collagen and negative for type X collagen, except for the 5% O_2 hanging group of one biological replicate, after 21 days of chondrogenic differentiation. These results suggest the positive role of the hanging group and the 2% O_2 environment to promote type II collagen production.

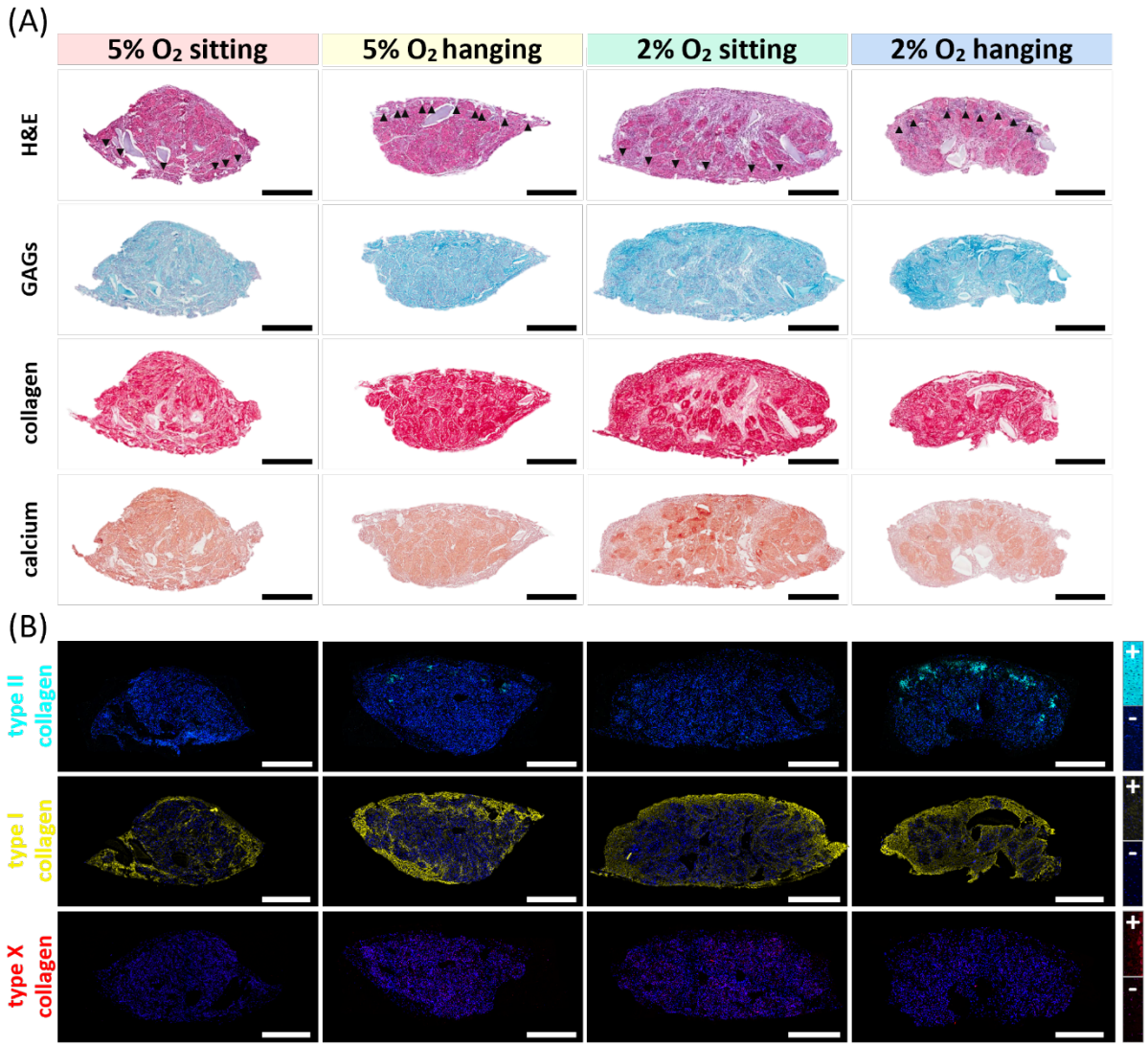

Fig. 5 Characterisation of the extracellular matrix (ECM) composition in scaled-up grafts. (A) Histology and (B) immunofluorescence staining panels of engineered tissues after 21 days of chondrogenic differentiation at 5% O_2 and 2% O_2, and in sitting and hanging orientations. Black arrows point at the anchoring points of the MEW fibres (only represented in the haematoxylin and eosin (H&E) staining). Nuclei are shown in dark blue. Scale bar = 500 µm. (For interpretation of the references to color in this figure legend, the reader is referred to the web version of this article.)

3.4. A MEW Mesh Can Direct Collagen Alignment Following Fusion of Cartilage Microtissues

Next, we assessed whether the MEW mesh and the hanging orientation could direct the orientation of the collagen fibre network using PLM. To assess if the spatial organisation of the engineered tissues was similar to native AC, the constructs (including the native AC positive control and the scaled-up graft fused in a nonadherent well negative control) were divided into 3 regions from the surface to the bottom of the tissue, and the collagen orientation distribution was assessed for each region. In native AC, a characteristic collagen network with fibres parallel to the top surface (0°) and fibres orientated perpendicular to the surface (90°) through the majority of the remaining tissue depth was observed (Fig. 6). As a result of its spherical geometry, microtissues placed into a nonadherent agarose well fused and generated a tissue with no preferential collagen fibre orientation (Fig. S3(B)). In the presence of a supporting MEW mesh, collagen fibres were aligned at approximately 0° at the top surface of the constructs, which closely

resembled the surface zone of native AC. In the middle region, fibres in the 2H group more coherently orientated in the same direction, with a group of fibres aligned at 45° to the surface. In contrast, all the other groups became less organised with depth, pointing to a greater level of stratification within the 2H group.

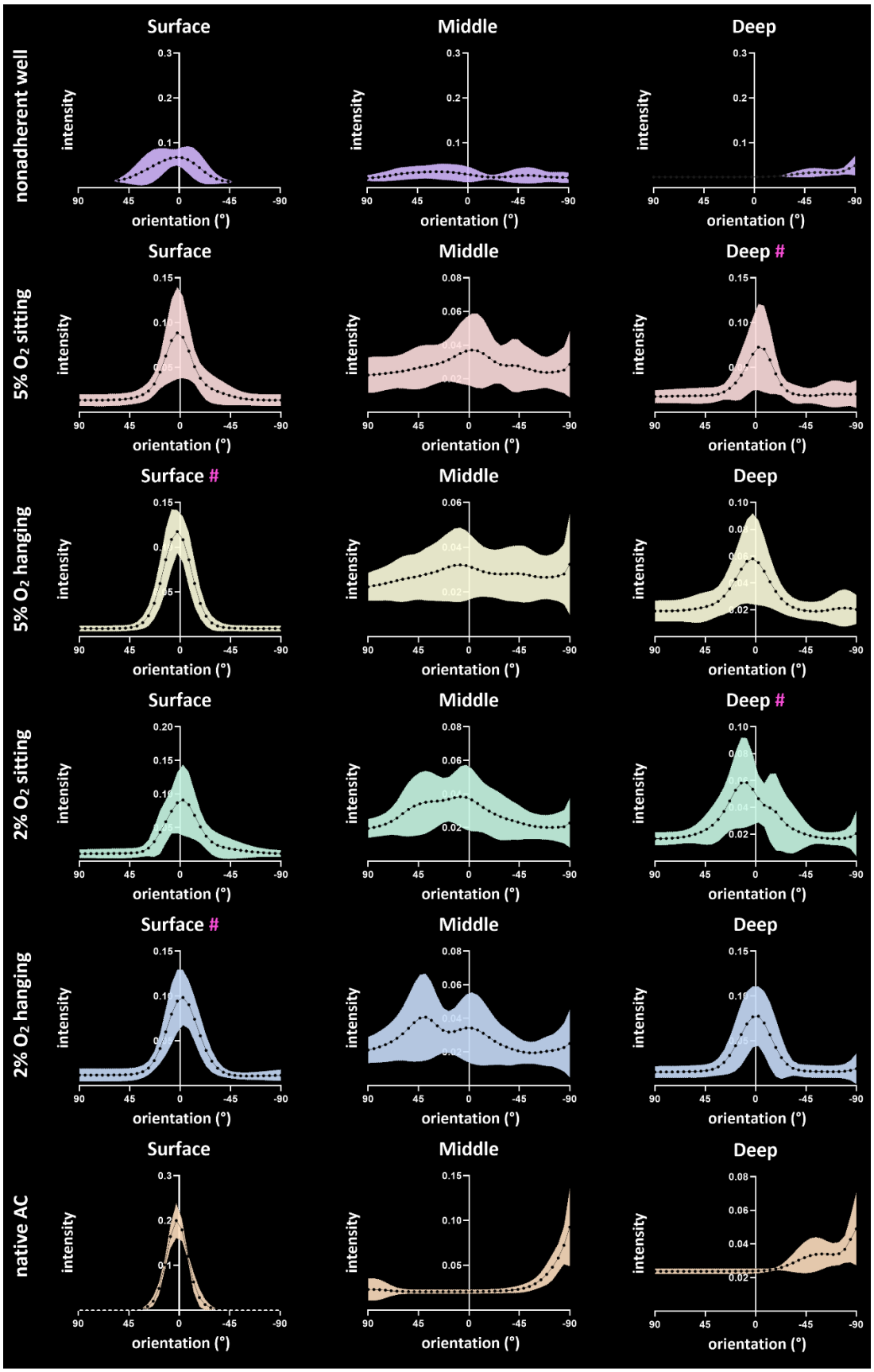

Fig. 6 Characterisation of the collagen network orientation in scaled-up grafts. Orientation distribution of collagen fibres in the surface, middle and deep regions of native articular cartilage (AC) and microtissues fused in nonadherent well or fused onto a MEW mesh at 5% O_2 and 2% O_2, and in sitting and hanging orientations. N = 12 (experimental groups) or 3 (controls). Data is represented as mean ± standard deviation. # indicated the presence of the MEW mesh in the corresponding region.

Further quantification of the collagen network within the pores of the MEW mesh showed that the dominant fibre orientation was not statistically different from that observed in the surface region of native AC (Fig. 7(A)). Interestingly, the fibre coherency, which reflects the variance of the dominant fibre orientation, was significantly higher (i.e. less variance) for the hanging groups compared to the sitting groups and was closer to native values (Fig. 7(B)). In addition, quantification of the dominant fibre orientation of the collagen fibres in the deeper regions of the engineered tissue distal to the MEW mesh in the 2H group was significantly higher than other groups (Fig. 7(C)). Hence, PLM quantification highlighted that our new fabrication approach, consisting of anchoring a MEW mesh with a layer of microtissues during the fusion process and then hanging the tissue from the mesh, yields an engineered tissue with a collagen network orientation displaying greater similarities with the native tissue. The hanging condition was then selected for further development.

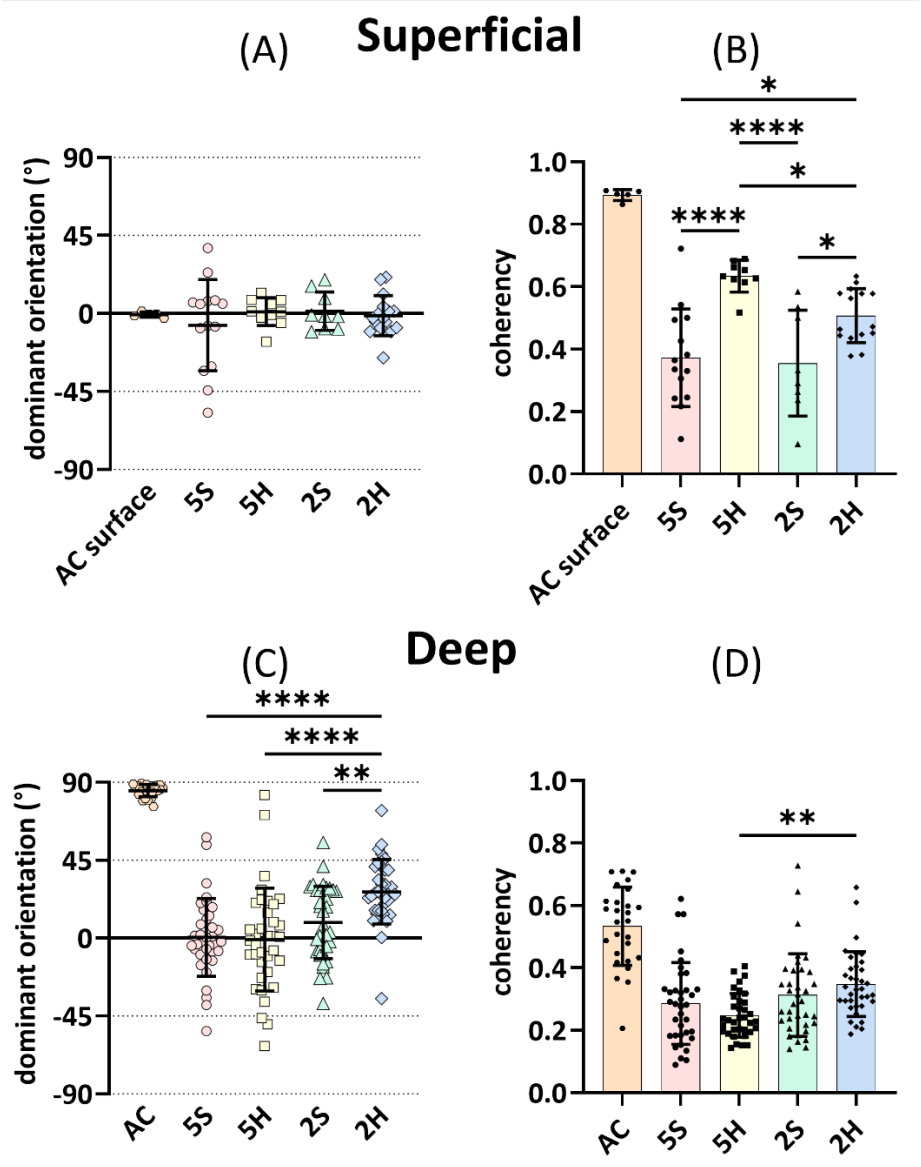

Fig. 7 Dominant orientation and coherency of collagen fibres in scaled-up grafts. The collagen fibre (A)&(C) dominant orientation and (B)&(D) coherency in (A)&(B) the superficial and (C)&(D) deep regions of native AC and AC surface, and engineered tissues differentiated at 5% O_2 (5) and 2% O_2 (2), and in sitting (S) and hanging (H) orientations. Note: for the hanging group, the superficial layer contains the MEW mesh, while for the sitting group, the MEW mesh is located within the deeper region of engineered grafts. All data is represented as individual data points and mean ± standard deviation. Normality was verified by Kolmogorov-Smirnov's test. Statistical differences were determined by one-way ANOVA test followed by Holm-Šídák's multiple comparison test. N ≥5 ((A)&(C)) or ≥27 ((B)&(D)). *p <0.05, **p <0.01, ****p <0.0001.

3.5. Modular Assembly of a Bilayered Hybrid Cartilaginous Tissue

As already demonstrated, chondrogenic differentiation under altered oxygen conditions yielded microtissues with distinct cartilaginous phenotypes. Microtissues differentiated at 2% O_2 produced GAG-rich ECM also containing type II collagen, while microtissues differentiated at 5% O_2 produced an ECM with a higher collagen-to-GAGs ratio. These different microtissues were next used as the building blocks for the different layers of AC in an attempt to mimic the ECM gradient found in the native tissue. Specifically, 5% O_2 differentiated microtissues were used to engineer the top region of AC, while 2% O_2 differentiated microtissues were used to engineer the bottom region of AC. Single microtissues were first primed for 7 days at both 5% O_2 or 2% O_2. At the 7-day timepoint, 5% O_2 microtissues were seeded onto the MEW mesh, followed 2 days later by 2% O_2 microtissues added on top of the first layer. As the mean microtissue diameter was 212 μm ± 20 μm, the pore size of the mesh was selected to be 200 μm × 200 μm. Two days after seeding the second layer of microtissues, the system was flipped upside down to hang the engineered tissues. Finally, the constructs were kept in TGF-β3 for 42 days at 5% O_2 (Fig. 8(A)). At day 11, prior to hanging the tissues, histological staining revealed that the two populations of microtissues (altered oxygen priming regimes) were spatially patterned in a two-layer manner. The top layer of this hanging construct, corresponding to microtissues primed at 5% O_2, contained more GAGs than the bottom layer, corresponding to microtissues primed at 2% O_2 (likely due to the fact that the microtissues primed at 5% O_2 had spent an additional 2 days in culture). Histological analysis after 42 days of ECM maturation revealed a strong staining for GAGs, with no obvious gradient despite the pre-priming of the single microtissues (Fig. 8(B)). Intense staining for collagen deposition was observed, which also revealed only partial fusion of the microtissues. In general, the regions between the unfused microtissues appeared homogeneous, stained positive for collagen and contained chondrocyte-like cells embedded in ECM. Some weak staining for calcium deposition was observed next to unfused microtissues. The analysis of the different collagen subtypes by immunofluorescent staining demonstrated the presence of type I, II and X collagen. Type I collagen and type II collagen were homogeneously distributed throughout the engineered tissue, except at the centre core of the tissue, where type II collagen was absent. In contrast, type X collagen was mainly observed at the centre of the tissue after 42 days of chondrogenic differentiation.

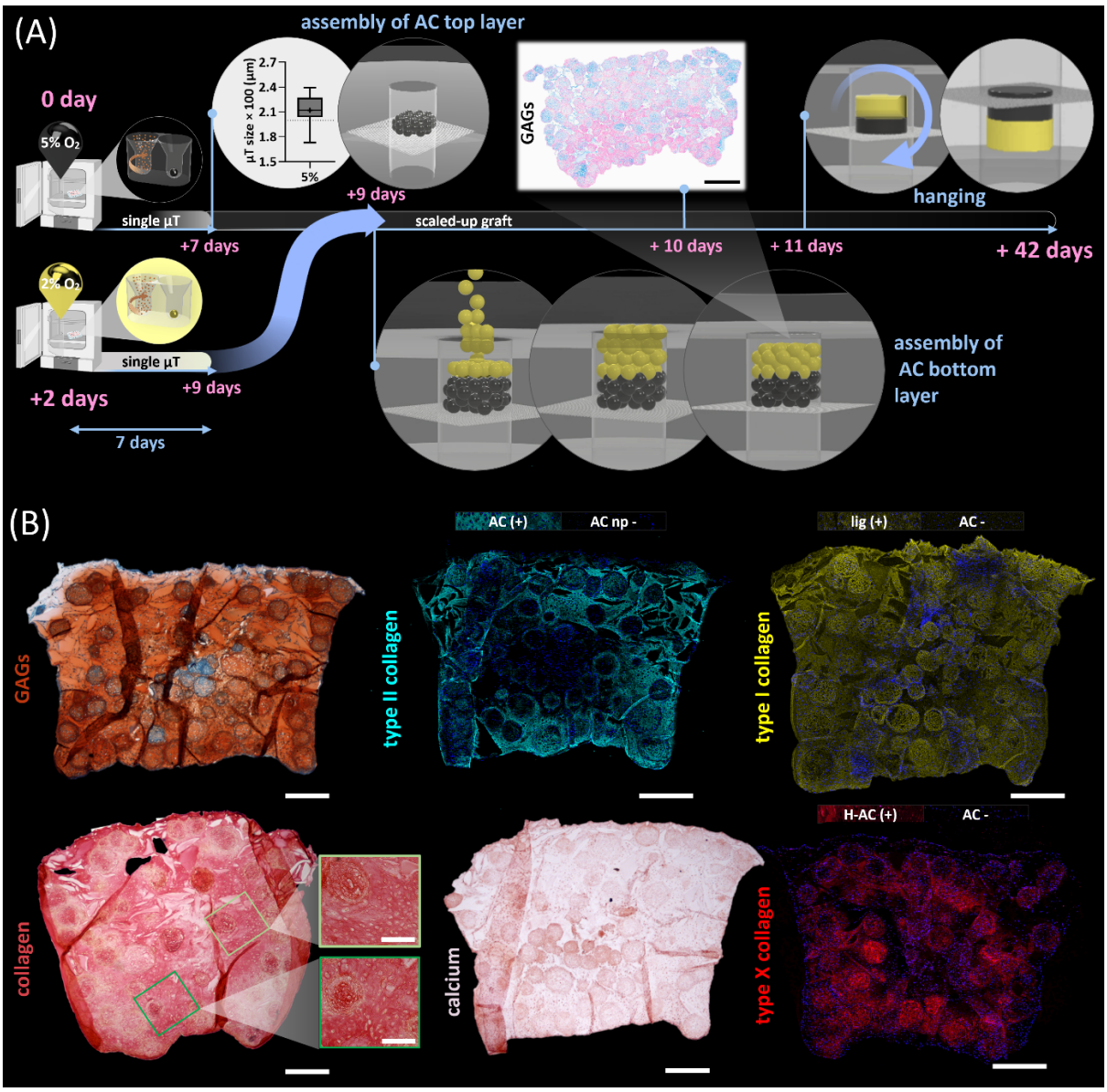

Fig. 8 Assembly of bilayered scaled-up graft and ECM characterisation. (A) Schematic representing the different steps of the bilayered scaled-up graft fabrication. Size of 7-day-old microtissues is represented as min to max box whiskers plot. Line represents median and dashed line represents the selected printing MEW pore size. N = 8. Histology stain of GAGs after 10 days of culture (one day after seeding the second layer of microtissues). Scale bar = 500 μm. (B) Histology and immunofluorescence stain of the bilayered graft after 42 days of chondrogenic differentiation. Scale bar = 500 μm or 200 μm (magnification). Nuclei are shown in dark blue. lig: ligament; H-AC: hypertrophic articular cartilage. (For interpretation of the references to color in this figure legend, the reader is referred to the web version of this article.)

4. Discussion

This study demonstrated that hMSC-derived microtissues with distinct cartilaginous phenotypes can be engineered by altering environmental oxygen levels. Lower oxygen levels (2% O_2) promoted the production of GAGs while maintaining type II collagen synthesis. In addition, only one week of 2% oxygen priming was necessary to generate microtissues containing more GAGs, motivating their use as biological building blocks for the biofabrication of spatially heterogeneous tissues. As a means of engineering an AC graft with both a predefined geometry and zonal organisation, a novel modular assembly method that integrates cartilaginous microtissues and a MEW mesh was developed. Using this approach, it was possible to spatially pattern microtissues containing distinct levels of GAGs into a supporting MEW mesh, enabling the generation of a scaled-up graft. Such approaches hold great potential for fabricating complex tissues with biomimetic composition and collagen fibre organisation.

Low oxygen conditions (2% O_2) significantly increased GAG production but had no negative effect on total collagen production. These results confirm the beneficial role of hypoxia for chondrogenesis of hMSCs [51, 52]. The transcription factor HIF-1α has been identified as a key mediator of chondrogenesis in low oxygen environments [53], regulating chondrocyte differentiation, proliferation and survival, and supporting ECM deposition [54, 55]. Local oxygen levels also influenced the collagen-to-GAG ratio, with microtissues differentiated at 5% O_2 more similar in composition to the surface region of native AC (Fig. S7(A)), where high levels of oxygen are found [25]. An analysis of donor-donor variability also suggests that lower oxygen conditions are particularly beneficial for MSCs with a lower inherent chondrogenic potential (compared to that observed at 5%) and could be a robust inducer of chondrogenesis (Fig. S7(B)). In line with this hypothesis, a similar trend was previously observed with the differentiation of hMSCs and human ACPs, where clones with inherent low-GAG production levels were significantly more responsive to low oxygen conditions [36]. In addition, characterisation of collagen subtypes by immunofluorescence staining confirmed the generation of cartilage with greater type II collagen accumulation under such low oxygen conditions. No signs of early hypertrophy, characterised by the presence of type X collagen, were visible which is consistent with previous findings in hypoxic conditions [56]. As MSCs have the inherent tendency to undergo hypertrophy and progress along the endochondral pathway [57], further long-term studies are needed to confirm whether this tendency is delayed or at best suppressed. In addition, further analysis of the phenotype (e.g. *via* RNA sequencing) of microtissues generated under altered oxygen environments is warranted.

From a tissue engineering point of view, such phenotypically distinct microtissues can be used as biological building blocks for the engineering of zonally organised tissue, in particular to recapitulate the gradients in biochemical composition seen in native AC. While different oxygen levels can easily be set for the culture of individual microtissues, spatial variation in oxygen develop during the culture of larger grafts. In an attempt to address this challenge, microtissues were exposed to temporal variations of oxygen, beginning with exposure to 2% O_2 for the first 7 days, and then switched to 5% O_2 for 14 days (termed '2–5%'), to assess whether the effect of short-term exposure to low oxygen can be maintained once subsequently exposed to higher oxygen levels. In terms of GAG production, microtissues from the 2–5% group outperformed the 2% and 5% groups, highlighting the potential of varying oxygen exposure to be used as building blocks for the deeper regions of AC. During cartilage development and tissue maturation, levels of oxygen vary with the developmental stage (hypoxia promotes cell proliferation and

oxygenation promotes organogenesis) and the tissue demand (mechanical loading, circadian rhythm, aging) [27, 58, 59]. In another study, short oxygen priming did not promote the chondrogenesis of cell-laden microsphere hydrogels. However, cell-cell and cell-matrix interactions, which drive chondrogenesis, are different in such scaffolds systems [60].

An in-house modular assembly system was then fabricated using a MEW mesh and agarose well. The agarose, gelled in presence of positive PDMS inserts, formed a seeding well with easily adaptable diameter, removing the need to use commercially available inserts to seed the microtissues onto the MEW mesh [21]. The MEW mesh served as the bottom of the agarose well to collect and integrate with the seeded microtissues. Success of this modular assembly strategy relies in part on the ability to generate meshes with highly accurate dimensions that can retain seeded microtissues. Hence, the use of melt electrowriting allowed the printing of meshes with well-defined box-like pore dimensions. Previous studies on the modular assembly of biosheets have found that the resulting construct contains ~2% polymeric material, with MEW scaffolds porosity of 80–98% [13, 17]. In this study, the MEW mesh was six-layer thick, while the resulting single-layered grafts were approximately 1.5 mm thick. Thus, this new modular approach can yield hybrid cartilage grafts with a minimal volume of synthetic biomaterial, especially when compared with FDM approaches [61]. Minimisation of the presence of PCL, even though it has already been used in Food and Drug Administration-approved therapeutics, is anticipated to favour clinical translation and biosafety [62].

Integrating cartilage microtissues into a MEW mesh was found to prevent cell mediated contraction of the final construct whilst simultaneously supporting chondrogenesis and graft development. After 21 days of chondrogenic differentiation, limited contraction of the fused graft was observed (graft dimensions were approximately 2.5 mm × 1.5 mm) even though only the bottom part of the construct was maintained by the MEW mesh [10, 13, 21]. In a previous study, adipose-derived stem cells were seeded in PCL buckyballs used to fabricate hybrid spheroids with consistent diameter [63]. While tissue contraction was attenuated by the incompressible volume of the buckyball “cage”, chondrogenesis and fusion of these hybrid tissues were not hampered, pointing to the utility of such supporting frameworks in the development of engineered tissues [64]. Here the MEW mesh-bottomed agarose well allowed both sides of the tissue, top and bottom, to be exposed to culture media. As the construct was not placed on culture plastic, diffusion of nutrients from both surfaces likely supported more homogeneous tissue development. Finally, the MEW mesh was entrapped within the secreted ECM but cells did not migrate beyond the mesh as previously observed with microtissues seeded on a nylon mesh, which contributed to the thickening of the tissue by 40% [10]. The fibronectin coating of the MEW fibres could contribute to enhancing cell attachment to the MEW surface [50].

Allowing the microtissues to hang from the MEW mesh was found to support type II collagen deposition and to significantly increase the coherency (less variation) of collagen fibres in presence of the mesh, closer to native values. As previously demonstrated, the MEW fibres were found to guide the orientation of newly synthesised collagen fibres [18, 19]. The collagen orientation distribution revealed that the 2H group (hanging orientation fabricated with microtissues differentiated at 2% O_2) contained fibres that started to orientate at 45° to the surface moving into the tissue depth, their dominant orientation being significantly different to that in the other groups. Collagen fibres in contact with the MEW fibres were predominantly orientated parallel to the surface in all groups, but the fibre coherency of the hanging groups was higher than the sitting groups. These results suggest that the combination of the physical constraints provided by the MEW mesh,

coupled with allowing the engineered tissue to hang in culture, yields a tissue that tends to more closely resemble native tissue.

To mimic the GAG gradient found in native AC, microtissues differentiated at 5% O_2 and 2% O_2 were then used to engineer the surface and deeper regions of the tissue. Despite only partial fusion of the microtissues, cells, most likely from the microtissue surface [65], were able to migrate outside of the microtissues and fill the inter-microtissue space with ECM rich in GAGs and type I, II and X collagen. In addition, no signs of tissue necrosis were observed (Fig. S8). In a similar study, millimetre-thick biosheets underwent core necrosis, but these engineered constructs were cultured under normoxic conditions (21% O_2) [10]. The initial layering of distinct microtissue populations was not visible after 42 days of culture. While the microtissues were initially phenotypically distinct, the absence of a biomimetic gradient in GAGs in the final tissue may be due to the continued deposition of extracellular matrix components with time in culture. Spatial variations in regulatory cues within such large, engineered grafts (e.g. oxygen, growth factors) also likely play a role in determining the long-term development of the graft [66]. A more detailed quantification of the composition in each region of the engineered graft would provide further insights into these phenotypical changes. In another study, sequentially assembled chondrogenic and osteogenic microtissue populations were able to maintain their layered organisation in culture, but 14-day-old microtissues were used as the second layer which were only maintained for further 8 days of culture, which might be too short to observe the remodelling of these slow-fusing microtissue building units [67]. Further work is required to identify the optional time periods microtissues should be independently cultured before they are combined with other microtissues to allow them not only to fuse but to maintain their desired phenotype in long-term culture. Embedding microtissue populations in supporting scaffolds or hydrogels, or the use of perfusion bioreactor systems could also be explored to modulate oxygen and nutrient gradients in large engineered tissues [68, 69].

It is worth mentioning that this novel modular assembly method holds the potential to engineer spatially complex and heterogeneous tissues with minimal use of foreign biomaterials. Microtissues were pipetted in the MEW mesh-bottomed well and arranged inside each pore as media was drained through the mesh. The manual nature of this process could contribute to some of the observed differences in tissue development using cells from different donors (Fig. S5). Superior complexity, efficiency and reliability could result from the implementation of bioprinting [70-72] and/or robotic bioassembly approaches [73, 74]. Aspiration-assisted bioprinting, even in combination with array fabrication of microtissues [44], and fluidic-based singularisation and injection modules, integrated to a commercial 3D printer, demonstrated precise positioning of individual microtissues in a 3D printed scaffold [75, 76]. While the MEW mesh improves the handleability of the graft [77], other specifications like mechanical integrity, surface lubrication, graft fixation and integration with surrounding tissues should also be considered [12]. In the future we will also explore the use of co-cultures of chondrocytes and MSCs [78, 79], or articular cartilage progenitor cells [69], to address the challenge of engineering more hyaline-like cartilage microtissues rich in type II collagen. Finally, further *in vitro* and *in vivo* studies are necessary to assess the effect of matrix maturation and (re)modelling on the biomechanical properties of the engineered tissue and the effect of the MEW mesh degradation on the regenerative potential of the engineered graft.

5. Conclusions

The results of this study confirm the beneficial role of hypoxia on chondrogenesis of hMSCs. Both 5% and 2% O_2 – oxygen representative of the superficial and deep zones of native articular cartilage, respectively – supported microtissue formation and type II collagen deposition. Notably, GAGs synthesis was significantly elevated under 2% O_2 compared to 5% O_2. Among, the various oxygen tensions and culture orientations examined, the 2% O_2 hanging culture (2H) conditions yielded greater type II collagen accumulation. Furthermore, the hanging orientation promoted greater collagen fibre alignment within the MEW mesh, more closely mimicking the structural characteristics of native articular cartilage than the sitting orientation. Finally, the modular assembly of distinct microtissue populations onto a MEW mesh facilitated the formation of a bilayered construct exhibiting an initial GAG gradient, although further investigation is required to assess the long-term maturation and stability of these engineered tissues.

CRediT authorship contribution statement

Nadia Rodriguez: Writing – review & editing, Writing – original draft, Visualization, Validation, Methodology, Investigation, Formal analysis, Data curation, Conceptualization. **Inês F. Gonçalves**: Writing – review & editing, Resources. **Tom Hodgkinson**: Writing – review & editing, Resources. **Fergal J. O'Brien**: Writing – review & editing, Funding acquisition. **Daniel J. Kelly**: Writing – review & editing, Supervision, Funding acquisition, Conceptualization.

Author statement

All authors have approved the manuscript and agree with its submission to *Biomaterials Advances*. We confirm that the work is original and that neither the manuscript nor any parts of its content are currently under consideration for publication with or published in another journal.

Funding sources

This work was supported by Taighde Éireann - Research Ireland [12/RC/2278_2]; and by the European Regional Development Fund and Taighde Éireann - Research Ireland under Ireland's European Structural and Investment Fund.

Declaration of competing interest

The authors declare no conflict of interest.

Acknowledgements

Authors would like to thank Prof. John M. O'Byrne, National Orthopaedics Hospital Cappagh, Dublin, Ireland. SEM was carried out at the Advanced Microscopy Laboratory (AML), Trinity College Dublin, Dublin, Ireland. The AML is an SFI supported imaging and analysis centre, part of the CRANN Institute and affiliated to the AMBER centre.

Appendix A Supplementary data

Table S1 Immunofluorescent staining protocol.

Controls	**(-)**	incubation in [3]BB as I^{ary} antibody	[4]AC	ligament or AC with BB as I^{ary} antibody	AC
	+		ligament	AC	hypertrophic AC
II^{ary} antibody		goat anti-rabbit – 1:250 A11037 (Invitrogen)	donkey anti-rabbit – 1:500 ab150075 (abcam)	donkey anti-mouse – 1:500 A21203 (Invitrogen)	donkey anti-mouse – 1:200 A21203 (Invitrogen)
I^{ary} antibody		anti-fibronectin – 1:200 ab23751 (abcam)	anti-type I collagen – 1:500 ab138492 (abcam)	anti-type II collagen – 1:100 sc-52658 (Santa Cruz Biotechnology)	anti-type X collagen – 1:50 14-9771-82 (Invitrogen)
Blocking buffer		10% v/v goat serum (Merck) + 1% w/v bovine serum albumin (Merck) in 1X PBS 1 h [1]RT [2]HC	10% v/v donkey serum (abcam) + 1% w/v bovine serum albumin (Merck) in 1X PBS		
Antigen retrieval		_	hyaluronidase – 4,000 U/mL 45 min 37 °C HC (Merck)		
			pronase – 35 U/mL 25 min 37 °C HC (Merck)		pronase – 3.5 U/mL 25 min 37 °C, HC (Merck)
Stain		fibronectin	type I collagen	type II collagen	type X collagen

[1]RT: room temperature; [2]HC: humidity chamber; [3]BB: blocking buffer; [4]AC: articular cartilage.

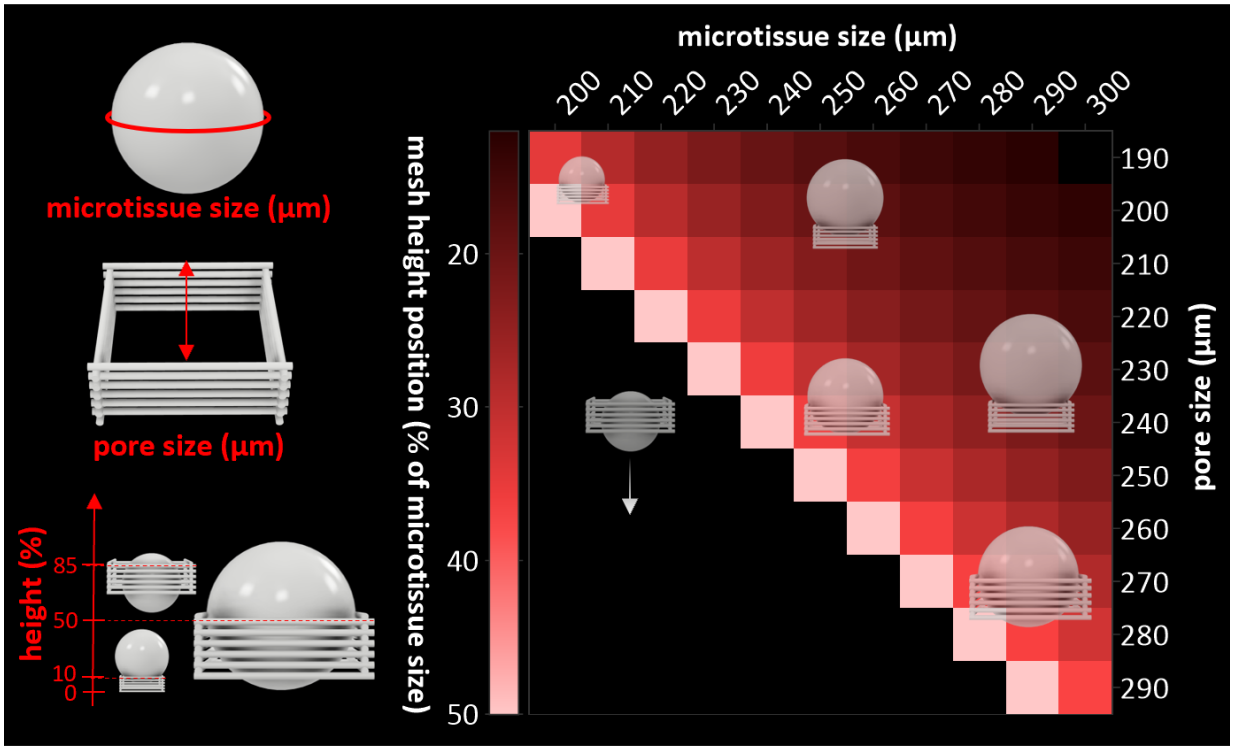

Fig. S1 Chart of the relative variations of mesh height position to microtissue size and pore size.

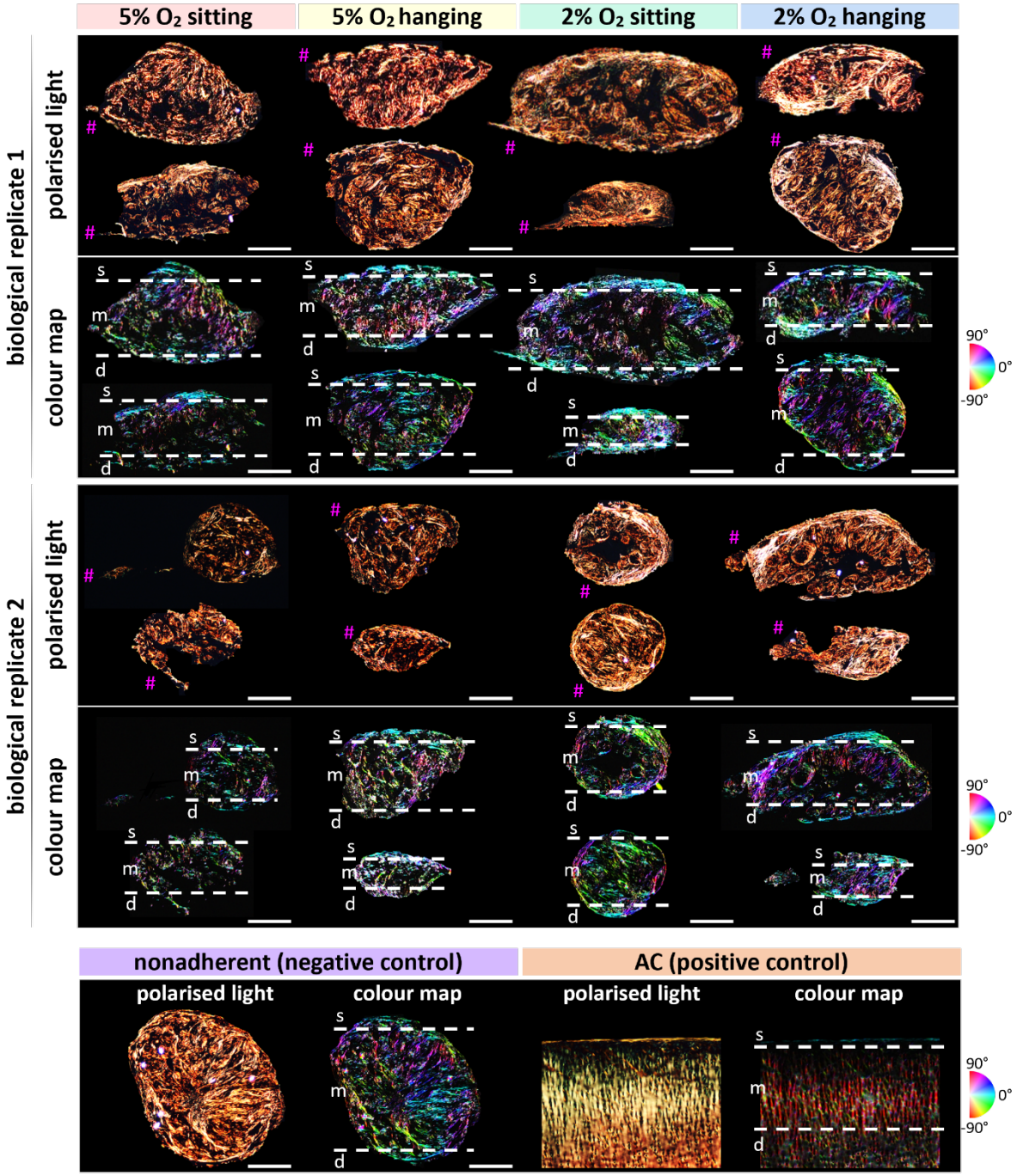

Fig. S2 Panel of polarised light and colour map images used to characterise the organisation of the collagen network in experimental groups (5% O_2 and 2% O_2, and in sitting and hanging orientations) and controls. #: position of the MEW mesh; s: superficial region; m: middle region; d: deep region. Scale bar = 500 μm.

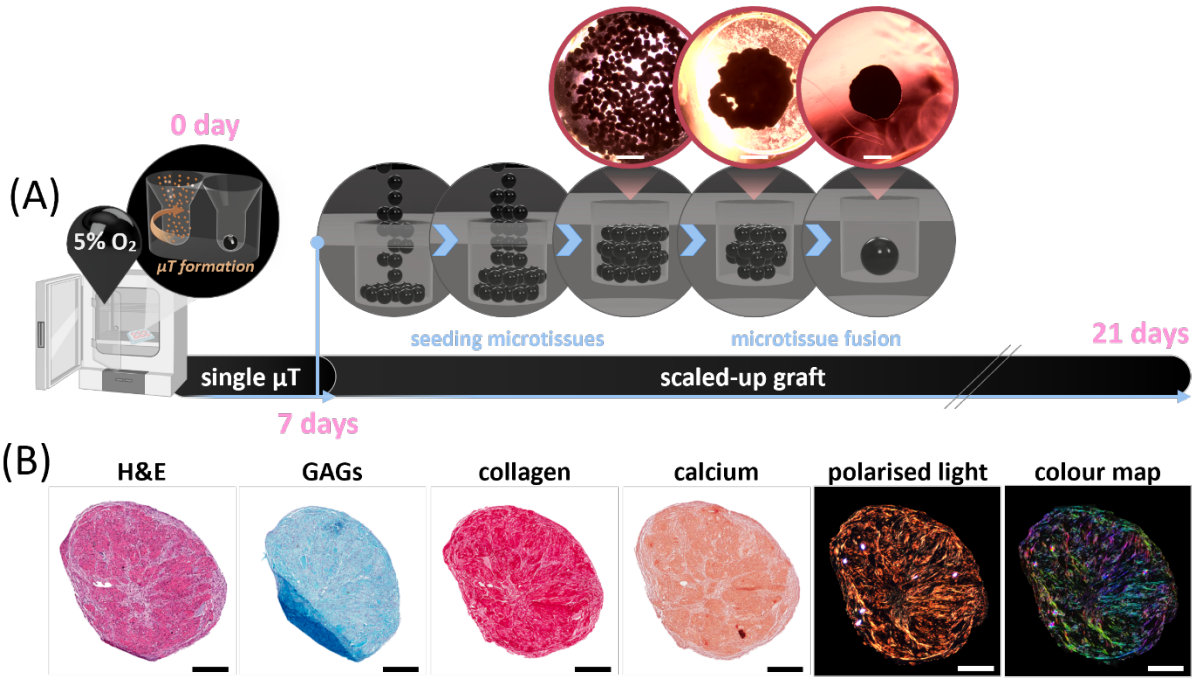

Fig. S3 Microtissue fusion in nonadherent agarose well. (A) Schematic and pictures of the fabrication steps of scaled-up grafts using a nonadherent agarose well (control). Scale bar = 1 mm. μT: microtissue. (B) Characterisation of the control graft extracellular matrix and collagen fibre orientation. Scale bar = 300 μm. H&E: haematoxylin and eosin; GAG: glycosaminoglycans.

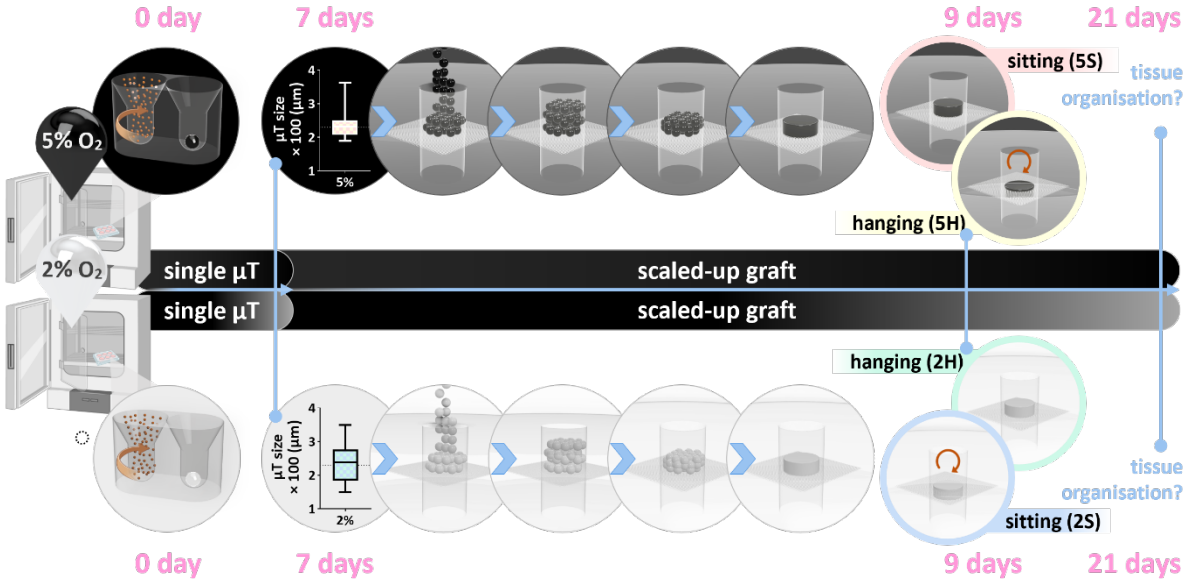

Fig. S4 Schematic representing the assembly steps of the sitting (S) and hanging (H) groups both fabricated at 5% O_2 (5) or 2% (2) O_2. Size of 7-day-old microtissues is represented as min to max box whiskers plot. Line represents median and dashed line represents the selected printing MEW pore size. N = 12.

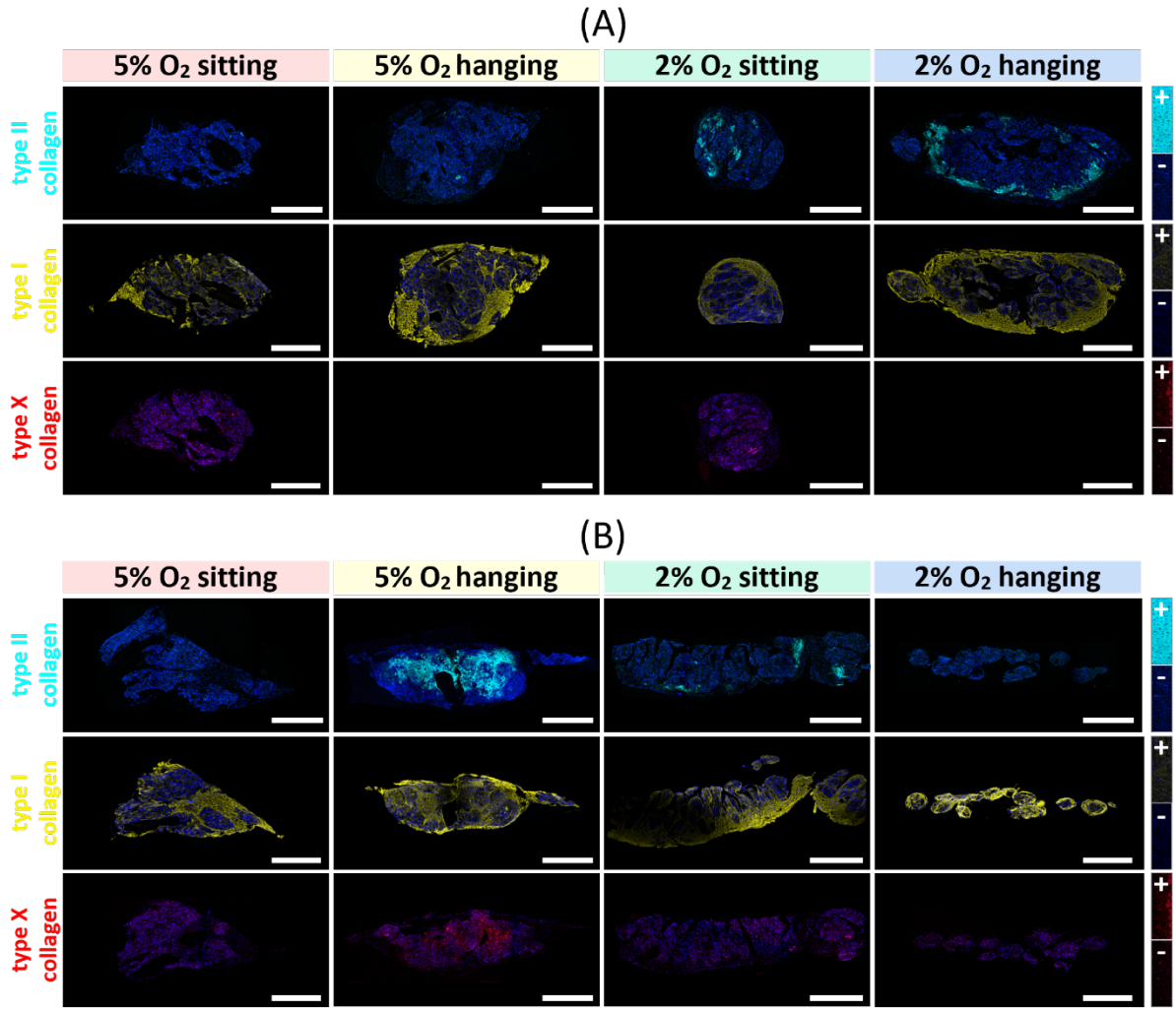

Fig. S5 Characterisation of the extracellular matrix composition in scaled-up grafts. (A)&(B) Immunofluorescence stain panels of biological replicates. Engineered tissues were differentiated for 21 days at 5% O_2 and 2% O_2, and in sitting and hanging orientations. Nuclei are shown in dark blue. Scale bar = 500 µm. (+): positive control; -: negative control.

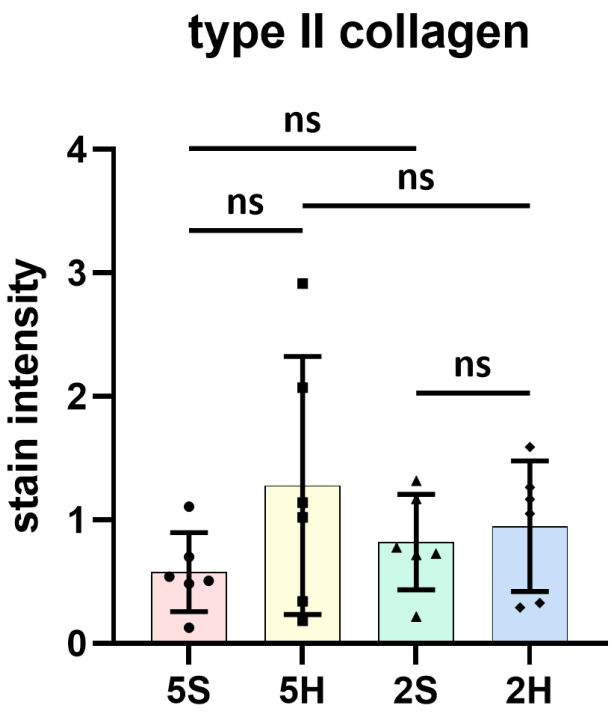

Fig. S6 Type II collagen stain intensity quantification of engineered tissues after 21 days of chondrogenic differentiation at 5% O_2 (5) and 2% O_2 (2), and in sitting (S) and hanging (H) orientations. All data is represented as mean ± standard deviation. Normality was verified by Shapiro-Wilk's test. Statistical differences were determined by one-way ANOVA test with Holm-Šídák's multiple comparison test. ns: not significant.

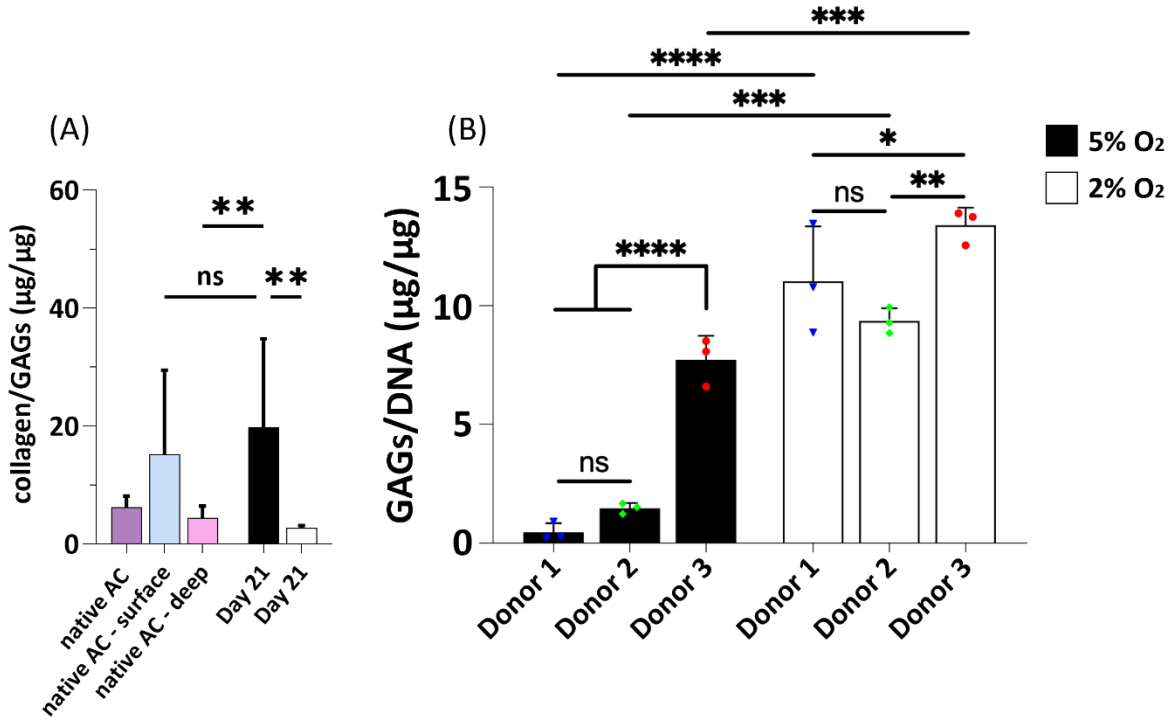

Fig. S7 Influence of low oxygen environment during chondrogenic differentiation of hMSC-derived microtissues. Biochemical analysis of (A) the collagen-to-GAGs ratio of native human articular cartilage and engineered chondrogenic microtissues (day 21) and (B) the GAGs normalised to DNA inter-donor variability (day 21). All data is represented as mean ± standard deviation and individual data points. Statistical differences were determined by one-way ANOVA test with Holm-Šídák's multiple comparison test ((A)) and by two-way ANOVA test with Holm-Šídák's multiple comparison test. N ≥ 6 ((A)) and 3 ((B)). ns denotes not significant, * denotes p <0.05, ** denotes p <0.01, *** denotes p<0.001, **** denotes p <0.0001. DNA: deoxyribonucleic acid; AC: articular cartilage.

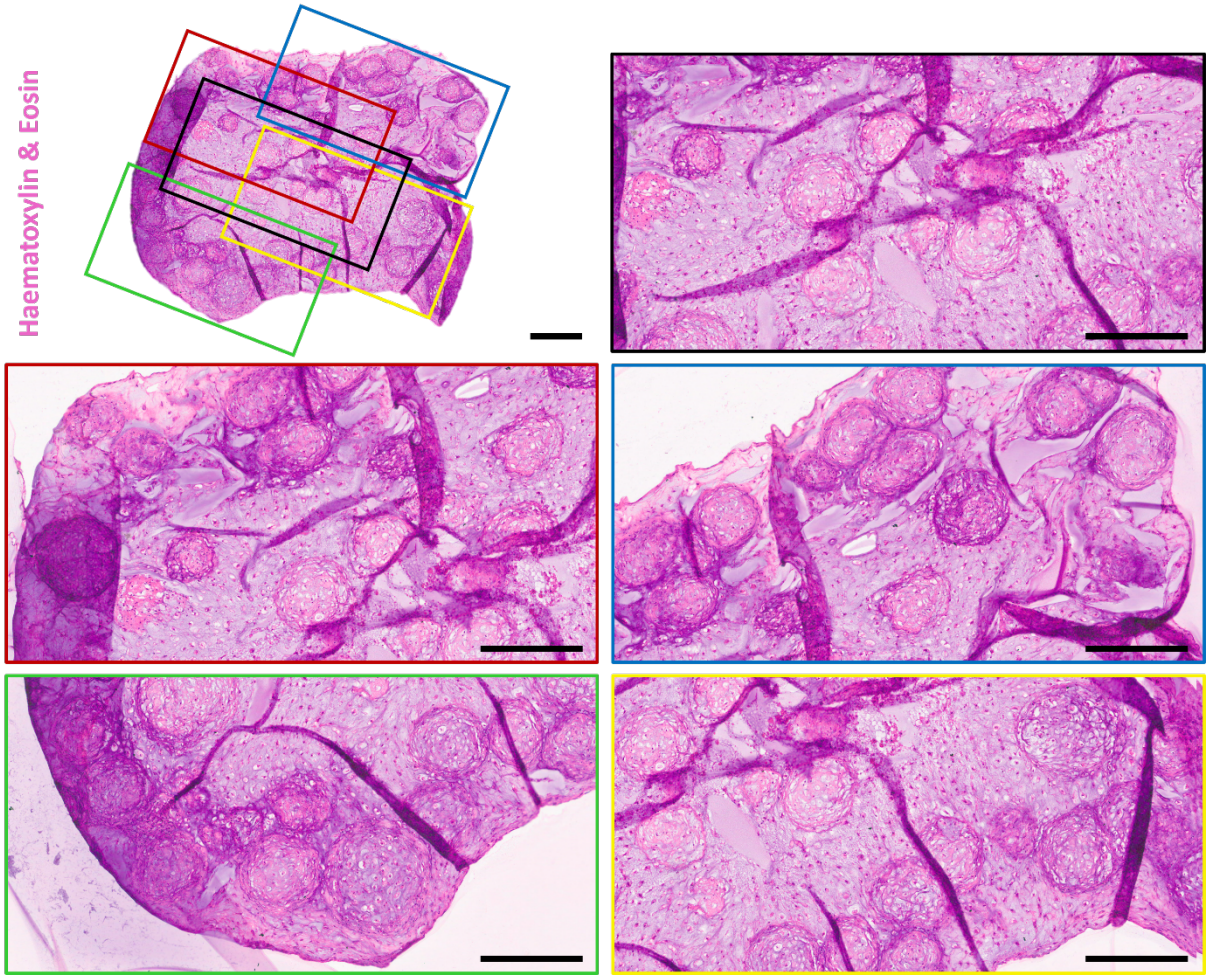

Fig. S8 Histology stain of the bilayered after 42 days of chondrogenic differentiation. Scale bar = 500 μm or **3**00 μm (magnification).

References

[1] J.M. Oliveira, V.P. Ribeiro, R.L. Reis, Advances on gradient scaffolds for osteochondral tissue engineering, Progress in Biomedical Engineering 3(3) (2021) 033001. https://dx.doi.org/10.1088/2516-1091/abfc2c.

[2] M. Wang, Y. Wu, G. Li, Q. Lin, W. Zhang, H. Liu, J. Su, Articular cartilage repair biomaterials: strategies and applications, Materials Today Bio 24 (2024) 100948. https://doi.org/10.1016/j.mtbio.2024.100948.

[3] Y. Chen, Y. Le, J. Yang, Y. Yang, X. Feng, J. Cai, Y. Shang, S. Sugiarto, Q. Wei, D. Kai, L. Zheng, J. Zhao, 3D Bioprinted Xanthan Hydrogels with Dual Antioxidant and Chondrogenic Functions for Post-traumatic Cartilage Regeneration, ACS Biomater Sci Eng 10(3) (2024) 1661-1675. https://doi.org/10.1021/acsbiomaterials.3c01636.

[4] Y. Wang, Y. Xu, G. Zhou, Y. Liu, Y. Cao, Biological Evaluation of Acellular Cartilaginous and Dermal Matrixes as Tissue Engineering Scaffolds for Cartilage Regeneration, Front Cell Dev Biol 8 (2020) 624337. https://doi.org/10.3389/fcell.2020.624337.

[5] S. Muthu, J.V. Korpershoek, E.J. Novais, G.F. Tawy, A.P. Hollander, I. Martin, Failure of cartilage regeneration: emerging hypotheses and related therapeutic strategies, Nat Rev Rheumatol 19(7) (2023) 403-416. https://doi.org/10.1038/s41584-023-00979-5.

[6] M.W. Laschke, M.D. Menger, Life is 3D: Boosting Spheroid Function for Tissue Engineering, Trends in Biotechnology 35(2) (2017) 133-144. https://doi.org/10.1016/j.tibtech.2016.08.004.

[7] G. Ofek, C.M. Revell, J.C. Hu, D.D. Allison, K.J. Grande-Allen, K.A. Athanasiou, Matrix development in self-assembly of articular cartilage, PLoS One 3(7) (2008) e2795. https://doi.org/10.1371/journal.pone.0002795.

[8] L. De Moor, E. Beyls, H. Declercq, Scaffold Free Microtissue Formation for Enhanced Cartilage Repair, Ann Biomed Eng 48(1) (2020) 298-311. https://doi.org/10.1007/s10439-019-02348-4.

[9] F.D. Spagnuolo, G.S. Kronemberger, K.J. Storey, D.J. Kelly, The maturation state and density of human cartilage microtissues influence their fusion and development into scaled-up grafts, Acta Biomaterialia 194 (2025) 109-121. https://doi.org/10.1016/j.actbio.2025.01.024.

[10] Q.B. Le, H. Ezhilarasu, W.W. Chan, A.T. Patra, P. Murugan, S.A. Venkatesh, Y.K. Tay, S.R. Lim, A.A. Abdul Rahim, J.S.Z. Lee, X. Bi, D. Choudhury, A platform for Bioengineering Tissue Membranes from cell spheroids, Materials Today Bio 31 (2025). https://doi.org/10.1016/j.mtbio.2025.101526.

[11] N.V. Kosheleva, Y.M. Efremov, B.S. Shavkuta, I.M. Zurina, D. Zhang, Y. Zhang, N.V. Minaev, A.A. Gorkun, S. Wei, A.I. Shpichka, I.N. Saburina, P.S. Timashev, Cell spheroid fusion: beyond liquid drops model, Sci Rep 10(1) (2020) 12614. https://doi.org/10.1038/s41598-020-69540-8.

[12] B.S. Schon, G.J. Hooper, T.B. Woodfield, Modular Tissue Assembly Strategies for Biofabrication of Engineered Cartilage, Ann Biomed Eng 45(1) (2017) 100-114. https://doi.org/10.1007/s10439-016-1609-3.

[13] G.N. Hall, A. Chandrakar, A. Pastore, K. Ioannidis, K. Moisley, M. Cirstea, L. Geris, L. Moroni, F.P. Luyten, P. Wieringa, I. Papantoniou, Engineering bone-forming biohybrid sheets through the integration of melt electrowritten membranes and cartilaginous microspheroids, Acta Biomater (2022). https://doi.org/10.1016/j.actbio.2022.10.037.

[14] K.F. Eichholz, D.A. Hoey, Mediating human stem cell behaviour via defined fibrous architectures by melt electrospinning writing, Acta Biomaterialia 75 (2018) 140-151. https://doi.org/10.1016/j.actbio.2018.05.048.

[15] J. Vazquez-Armendariza, R. Tejeda-Alejandre, A. Bahhurd, C.A. Rodriguez, D. Dean, Meltelectrowriting of Polycaprolactone Thin Membranes with High Porosity, Procedia CIRP, 2022, pp. 282–286. http://dx.doi.org/10.1016/j.procir.2022.06.051.
[16] A. Hrynevich, B.S. Elci, J.N. Haigh, R. McMaster, A. Youssef, C. Blum, T. Blunk, G. Hochleitner, J. Groll, P.D. Dalton, Dimension-Based Design of Melt Electrowritten Scaffolds, Small 14(22) (2018) e1800232. https://doi.org/10.1002/smll.201800232.
[17] P.D. Dalton, T.B.F. Woodfield, V. Mironov, J. Groll, Advances in Hybrid Fabrication toward Hierarchical Tissue Constructs, Advanced Science 7(11) (2020) 1902953. https://doi.org/10.1002/advs.201902953.
[18] X. Barceló, K.F. Eichholz, I.F. Gonçalves, O. Garcia, D.J. Kelly, Bioprinting of structurally organized meniscal tissue within anisotropic melt electrowritten scaffolds, Acta Biomaterialia 158 (2023) 216-227. https://doi.org/10.1016/j.actbio.2022.12.047.
[19] X. Barcelo, K. Eichholz, I. Goncalves, G.S. Kronemberger, A. Dufour, O. Garcia, D.J. Kelly, Bioprinting of scaled-up meniscal grafts by spatially patterning phenotypically distinct meniscus progenitor cells within melt electrowritten scaffolds, Biofabrication 16(1) (2023). https://doi.org/10.1088/1758-5090/ad0ab9.
[20] A. Dufour, X.B. Gallostra, C. O'Keeffe, K. Eichholz, S. Von Euw, O. Garcia, D.J. Kelly, Integrating melt electrowriting and inkjet bioprinting for engineering structurally organized articular cartilage, Biomaterials 283 (2022) 121405. https://doi.org/10.1016/j.biomaterials.2022.121405.
[21] R. McMaster, C. Hoefner, A. Hrynevich, C. Blum, M. Wiesner, K. Wittmann, T.R. Dargaville, P. Bauer-Kreisel, J. Groll, P.D. Dalton, T. Blunk, Tailored Melt Electrowritten Scaffolds for the Generation of Sheet-Like Tissue Constructs from Multicellular Spheroids, Adv Healthc Mater 8(7) (2019) e1801326. https://doi.org/10.1002/adhm.201801326.
[22] A.C. Daly, B.N. Sathy, D.J. Kelly, Engineering large cartilage tissues using dynamic bioreactor culture at defined oxygen conditions, J Tissue Eng 9 (2018) 2041731417753718. https://doi.org/10.1177/2041731417753718.
[23] S. Zhou, Z. Cui, J.P.G. Urban, Factors influencing the oxygen concentration gradient from the synovial surface of articular cartilage to the cartilage–bone interface: A modeling study, Arthritis & Rheumatism 50(12) (2004) 3915-3924. https://doi.org/10.1002/art.20675
[24] J.E. Lafont, Lack of oxygen in articular cartilage: consequences for chondrocyte biology, Int J Exp Pathol 91(2) (2010) 99-106. https://doi.org/10.1111/j.1365-2613.2010.00707.x.
[25] G. Pattappa, B. Johnstone, J. Zellner, D. Docheva, P. Angele, The Importance of Physioxia in Mesenchymal Stem Cell Chondrogenesis and the Mechanisms Controlling Its Response, International Journal of Molecular Sciences 20(3) (2019) 484. https://doi.org/10.3390/ijms20030484.
[26] M.J. Lammi, C. Qu, Regulation of Oxygen Tension as a Strategy to Control Chondrocytic Phenotype for Cartilage Tissue Engineering and Regeneration, Bioengineering 11(3) (2024) 211. https://doi.org/10.3390/bioengineering11030211.
[27] E. Zoneff, Y. Wang, C. Jackson, O. Smith, S. Duchi, C. Onofrillo, B. Farrugia, S.E. Moulton, R. Williams, C. Parish, D.R. Nisbet, L.M. Caballero-Aguilar, Controlled oxygen delivery to power tissue regeneration, Nat Commun 15(1) (2024) 4361. https://doi.org/10.3390/bioengineering11030211.
[28] R. Amarilio, S.V. Viukov, A. Sharir, I. Eshkar-Oren, R.S. Johnson, E. Zelzer, HIF1α regulation of Sox9 is necessary to maintain differentiation of hypoxic prechondrogenic cells during early skeletogenesis, Development 134(21) (2007) 3917-3928. https://doi.org/10.1242/dev.008441.
[29] X. Huang, Y. Hou, L. Zhong, D. Huang, H. Qian, M. Karperien, W. Chen, Promoted Chondrogenesis of Cocultured Chondrocytes and Mesenchymal Stem Cells under Hypoxia Using In-situ Forming Degradable Hydrogel Scaffolds, Biomacromolecules 19(1) (2018) 94-102. http://dx.doi.org/10.1021/acs.biomac.7b01271.

[30] E.J. Koay, K.A. Athanasiou, Hypoxic chondrogenic differentiation of human embryonic stem cells enhances cartilage protein synthesis and biomechanical functionality, Osteoarthritis and Cartilage 16(12) (2008) 1450-1456. https://doi.org/10.1016/j.joca.2008.04.007.
[31] H.C. Bae, H.J. Park, S.Y. Wang, H.R. Yang, M.C. Lee, H.-S. Han, Hypoxic condition enhances chondrogenesis in synovium-derived mesenchymal stem cells, Biomaterials Research 22(1) (2018) 28. https://doi.org/10.1186/s40824-018-0134-x.
[32] W.S. Khan, A.B. Adesida, T.E. Hardingham, Hypoxic conditions increase hypoxia-inducible transcription factor 2α and enhance chondrogenesis in stem cells from the infrapatellar fat pad of osteoarthritis patients, Arthritis Research & Therapy 9(3) (2007) R55. https://doi.org/10.1186/ar2211.
[33] A.B. Adesida, A. Mulet-Sierra, N.M. Jomha, Hypoxia mediated isolation and expansion enhances the chondrogenic capacity of bone marrow mesenchymal stromal cells, Stem Cell Research & Therapy 3(2) (2012) 9. https://doi.org/10.1186/scrt100.
[34] T.D. Bornes, N.M. Jomha, A. Mulet-Sierra, A.B. Adesida, Hypoxic culture of bone marrow-derived mesenchymal stromal stem cells differentially enhances in vitro chondrogenesis within cell-seeded collagen and hyaluronic acid porous scaffolds, Stem Cell Research & Therapy 6(1) (2015) 84. https://doi.org/10.1186/s13287-015-0075-4.
[35] S. Munir, C.B. Foldager, M. Lind, V. Zachar, K. Søballe, T.G. Koch, Hypoxia enhances chondrogenic differentiation of human adipose tissue-derived stromal cells in scaffold-free and scaffold systems, Cell and Tissue Research 355(1) (2014) 89-102. https://doi.org/10.1007/s00441-013-1732-5.
[36] D.E. Anderson, B.D. Markway, D. Bond, H.E. McCarthy, B. Johnstone, Responses to altered oxygen tension are distinct between human stem cells of high and low chondrogenic capacity, Stem Cell Res Ther 7(1) (2016) 154. https://doi.org/10.1186/s13287-016-0419-8.
[37] J. Bolander, C. Mota, H.W. Ooi, H. Agten, M.B. Baker, L. Moroni, F.P. Luyten, Bioinspired Development of an In Vitro Engineered Fracture Callus for the Treatment of Critical Long Bone Defects, Advanced Functional Materials 31(46) (2021).
[38] S. Sieber, M. Michaelis, H. Gühring, S. Lindemann, A. Gigout, Importance of Osmolarity and Oxygen Tension for Cartilage Tissue Engineering, Biores Open Access 9(1) (2020) 106-115. https://doi.org/10.1002/adfm.202104159.
[39] M. Kanichai, D. Ferguson, P.J. Prendergast, V.A. Campbell, Hypoxia promotes chondrogenesis in rat mesenchymal stem cells: A role for AKT and hypoxia-inducible factor (HIF)-1α, Journal of Cellular Physiology 216(3) (2008) 708-715. https://doi.org/10.1002/jcp.21446
[40] S.F. Carroll, C.T. Buckley, D.J. Kelly, Measuring and Modeling Oxygen Transport and Consumption in 3D Hydrogels Containing Chondrocytes and Stem Cells of Different Tissue Origins, Front Bioeng Biotechnol 9 (2021) 591126. https://doi.org/10.3389/fbioe.2021.591126.
[41] R. Burdis, G.S. Kronemberger, D.J. Kelly, Engineering High-Quality Cartilage Microtissues Using Hydrocortisone Functionalized Microwells, Tissue Engineering Part C: Methods 29(4) (2023) 121-133. https://doi.org/10.1089/ten.tec.2022.0181.
[42] J. Nulty, R. Burdis, D.J. Kelly, Biofabrication of Prevascularised Hypertrophic Cartilage Microtissues for Bone Tissue Engineering, Front Bioeng Biotechnol 9 (2021) 661989. https://doi.org/10.3389/fbioe.2021.661989.
[43] K.F. Eichholz, I. Gonçalves, X. Barceló, A.S. Federici, D.A. Hoey, D.J. Kelly, How to design, develop and build a fully-integrated melt electrowriting 3D printer, Additive Manufacturing 58 (2022) 102998. http://dx.doi.org/10.1016/j.addma.2022.102998.
[44] G. Nilsson Hall, I. Rutten, J. Lammertyn, J. Eberhardt, L. Geris, F.P. Luyten, I. Papantoniou, Cartilaginous spheroid-assembly design considerations for endochondral

ossification: towards robotic-driven biomanufacturing, Biofabrication 13(4) (2021) 045025. https://doi.org/10.1088/1758-5090/ac2208.
[45] W. Kafienah, T.J. Sims, Biochemical methods for the analysis of tissue-engineered cartilage, Methods Mol Biol 238 (2004) 217-30. https://doi.org/10.1385/1-59259-428-x:217.
[46] N.Y. Ignat'eva, N.A. Danilov, S.V. Averkiev, M.V. Obrezkova, V.V. Lunin, E.N. Sobol', Determination of hydroxyproline in tissues and the evaluation of the collagen content of the tissues, Journal of Analytical Chemistry 62(1) (2007) 51-57. https://doi.org/10.1134/S106193480701011X.
[47] R.W. Farndale, D.J. Buttle, A.J. Barrett, Improved quantitation and discrimination of sulphated glycosaminoglycans by use of dimethylmethylene blue, Biochimica et Biophysica Acta (BBA) - General Subjects 883(2) (1986) 173-177. https://doi.org/10.1016/0304-4165(86)90306-5.
[48] C.H. Zheng, M.E. Levenston, Fact versus artifact: avoiding erroneous estimates of sulfated glycosaminoglycan content using the dimethylmethylene blue colorimetric assay for tissue-engineered constructs, Eur Cell Mater 29 (2015) 224-36. https://doi.org/10.22203/ecm.v029a17.
[49] R. Burdis, X.B. Gallostra, D.J. Kelly, Temporal Enzymatic Treatment to Enhance the Remodeling of Multiple Cartilage Microtissues into a Structurally Organized Tissue, Adv Healthc Mater 13(3) (2024) e2300174. https://doi.org/10.1002/adhm.202300174
[50] D.E. Anderson, B.D. Markway, K.J. Weekes, H.E. McCarthy, B. Johnstone, Physioxia Promotes the Articular Chondrocyte-Like Phenotype in Human Chondroprogenitor-Derived Self-Organized Tissue, Tissue Eng Part A 24(3-4) (2018) 264-274. https://doi.org/10.1089/ten.tea.2016.0510.
[51] P. Giannoni, A. Crovace, M. Malpeli, E. Maggi, R. Arbicò, R. Cancedda, B. Dozin, Species Variability in the Differentiation Potential of in Vitro-Expanded Articular Chondrocytes Restricts Predictive Studies on Cartilage Repair Using Animal Models, Tissue Engineering 11(1-2) (2005) 237-248. https://doi.org/10.1089/ten.2005.11.237.
[52] W.A. Noort, M.I. Oerlemans, H. Rozemuller, D. Feyen, S. Jaksani, D. Stecher, B. Naaijkens, A.C. Martens, H.J. Bühring, P.A. Doevendans, J.P. Sluijter, Human versus porcine mesenchymal stromal cells: phenotype, differentiation potential, immunomodulation and cardiac improvement after transplantation, J Cell Mol Med 16(8) (2012) 1827-39. https://doi.org/10.1111/j.1582-4934.2011.01455.x.
[53] E. Duval, C. Baugé, R. Andriamanalijaona, H. Bénateau, S. Leclercq, S. Dutoit, L. Poulain, P. Galéra, K. Boumédiene, Molecular mechanism of hypoxia-induced chondrogenesis and its application in in vivo cartilage tissue engineering, Biomaterials 33(26) (2012) 6042-6051. https://doi.org/10.1016/j.biomaterials.2012.04.061.
[54] E. Schipani, Hypoxia and HIF-1α in chondrogenesis, Seminars in Cell & Developmental Biology 16(4) (2005) 539-546. https://doi.org/10.1016/j.semcdb.2005.03.003.
[55] X. Sun, Y. Wei, The role of hypoxia-inducible factor in osteogenesis and chondrogenesis, Cytotherapy 11(3) (2009) 261-267. https://doi.org/10.1080/14653240902824765.
[56] B.D. Markway, H. Cho, B. Johnstone, Hypoxia promotes redifferentiation and suppresses markers of hypertrophy and degeneration in both healthy and osteoarthritic chondrocytes, Arthritis Res. Ther. 15 (R92) (2013), doi:10.1186/ar4272.
[57] K. Futrega, P.G. Robey, T.J. Klein, R.W. Crawford, M.R. Doran, A single day of TGF-beta1 exposure activates chondrogenic and hypertrophic differentiation pathways in bone marrow-derived stromal cells, Commun Biol 4(1) (2021) 29. https://doi.org/10.1038/s42003-020-01520-0.
[58] S. Fathollahipour, Pritam S. Patil, Nic D. Leipzig, Oxygen Regulation in Development: Lessons from Embryogenesis towards Tissue Engineering, Cells Tissues Organs 205(5-6) (2018) 350-371. https://doi.org/10.1159/000493162.

[59] N. Rogers, Q.-J. Meng, Tick tock, the cartilage clock, Osteoarthritis and Cartilage 31(11) (2023) 1425-1436. https://doi.org/10.1016/j.joca.2023.05.010.
[60] G. Lindberg, A. Norberg, B. Soliman, T. Jüngst, K. Lim, G. Hooper, J. Groll, T. Woodfield, Fabrication of gelatin-heparin based cartilage models: enhancing spatial complexity through refinement of stiffness properties and oxygen availability, Frontiers in Biomaterials Science 3 (2024). https://doi.org/10.3389/fbiom.2024.1331032.
[61] R. Sinha, M. Camara-Torres, P. Scopece, E. Verga Falzacappa, A. Patelli, L. Moroni, C. Mota, A hybrid additive manufacturing platform to create bulk and surface composition gradients on scaffolds for tissue regeneration, Nat Commun 12(1) (2021) 500. https://doi.org/10.1038/s41467-020-20865-y.
[62] W. Guo, M. Chen, Z. Wang, Y. Tian, J. Zheng, S. Gao, Y. Li, Y. Zheng, X. Li, J. Huang, W. Niu, S. Jiang, C. Hao, Z. Yuan, Y. Zhang, M. Wang, Z. Wang, J. Peng, A. Wang, Y. Wang, X. Sui, W. Xu, L. Hao, X. Zheng, S. Liu, Q. Guo, 3D-printed cell-free PCL-MECM scaffold with biomimetic micro-structure and micro-environment to enhance in situ meniscus regeneration, Bioact Mater 6(10) (2021) 3620-3633. https://doi.org/10.1016/j.bioactmat.2021.02.019.
[63] O. Guillaume, O. Kopinski-Grunwald, G. Weisgrab, T. Baumgartner, A. Arslan, K. Whitmore, S. Van Vlierberghe, A. Ovsianikov, Hybrid spheroid microscaffolds as modular tissue units to build macro-tissue assemblies for tissue engineering, Acta Biomater 165 (2023) 72-85. https://doi.org/10.1016/j.actbio.2022.03.010.
[64] O. Kopinski-Grünwald, O. Guillaume, T. Ferner, B. Schädl, A. Ovsianikov, Scaffolded spheroids as building blocks for bottom-up cartilage tissue engineering show enhanced bioassembly dynamics, Acta Biomaterialia 174 (2024) 163-176. https://doi.org/10.1016/j.actbio.2023.12.001.
[65] R. Pan, C. Lin, X. Yang, Y. Xie, L. Gao, L. Yu, The influence of spheroid maturity on fusion dynamics and micro-tissue assembly in 3D tumor models, Biofabrication 16 (2024). https://doi.org/10.1088/1758-5090/ad4392.
[68] D.W. Chen, J. Y.; Kennedy, K. M.; Yeager, K.; Bernhard, J. C.; Ng J. J.; Zimmerman, B. K.; Robinson, S.; Durney, K. M.; Shaeffer, C.; Vila, O. F.; Takawira, C.; Gimble, J. M.; Guo, X. E.; Ateshian, G. A.; Lopez, M. J.; Eisig, S. B.; Vunjak-Novakovic, G. , Tissue engineered autologous cartilage-bone grafts for temporomandibular joint regeneration, Science Translational Medicicne 12(eabb6683) (2020). https://doi.org/10.1126/scitranslmed.abb6683.
[69] R. Levato, W.R. Webb, I.A. Otto, A. Mensinga, Y. Zhang, M. van Rijen, R. van Weeren, I.M. Khan, J. Malda, The bio in the ink: cartilage regeneration with bioprintable hydrogels and articular cartilage-derived progenitor cells, Acta Biomater 61 (2017) 41-53. https://doi.org/10.1016/j.actbio.2017.08.005.
[67] B.K. Babur, K. Futrega, W.B. Lott, T.J. Klein, J. Cooper-White, M.R. Doran, High-throughput bone and cartilage micropellet manufacture, followed by assembly of micropellets into biphasic osteochondral tissue, Cell Tissue Res 361(3) (2015) 755-68. https://doi.org/10.1007/s00441-015-2159-y.
[66] J. Malda, D.E. Martens, J. Tramper, C.A. van Blitterswijk, J. Riesle, Cartilage Tissue Engineering Controversy in the Effect of Oxygen, Critical Reviews in Biotechnology 23(3) (2003) 175–194.
[70] C.Y. Shen, Q.R. Zhou, X. Wu, X.Y. Han, Q. Zhang, X. Chen, Y.X. Lai, L. Bai, Y.Y. Jing, J.H. Wang, C.L. Wang, Z. Geng, J.C. Su, Accelerating cartilage regeneration with DNA-SF hydrogel sustained release system-based cartilage organoids, Mil Med Res 12(1) (2025) 39. https://doi.org/10.1186/s40779-025-00625-z.
[71] Z. Chen, H. Zhang, J. Huang, W. Weng, Z. Geng, M. Li, J. Su, DNA-encoded dynamic hydrogels for 3D bioprinted cartilage organoids, Mater Today Bio 31 (2025) 101509. https://doi.org/10.1016/j.mtbio.2025.101509.

[72] Z. Ma, Y. Wu, G. Li, J. Liu, Z. Geng, J. Su, Extracellular vesicles-loaded DNA hydrogels: A promising candidate for cartilage organoids engineering, Chemical Engineering Journal 477 (2023) 147146. https://doi.org/10.1016/j.cej.2023.147146.
[73] E. Vuille-Dit-Bille, D.V. Deshmukh, S. Connolly, S. Heub, S. Boder-Pasche, J. Dual, M.W. Tibbitt, G. Weder, Tools for manipulation and positioning of microtissues, Lab Chip 22(21) (2022) 4043-4066. https://doi.org/10.1039/D2LC00559J.
[74] I. Decoene, G. Nasello, R.F. Madeiro de Costa, G. Nilsson Hall, A. Pastore, I. Van Hoven, S. Ribeiro Viseu, C. Verfaillie, L. Geris, F.P. Luyten, I. Papantoniou, Robotics-Driven Manufacturing of Cartilaginous Microtissues for Skeletal Tissue Engineering Applications, Stem Cells Translational Medicine 13(3) (2024) 278-292. https://doi.org/10.1093/stcltm/szad091.
[75] N.V. Mekhileri, K.S. Lim, G.C.J. Brown, I. Mutreja, B.S. Schon, G.J. Hooper, T.B.F. Woodfield, Automated 3D bioassembly of micro-tissues for biofabrication of hybrid tissue engineered constructs, Biofabrication 10(2) (2018) 024103. https://doi.org/10.1088/1758-5090/aa9ef1.
[76] B. Ayan, N. Celik, Z. Zhang, K. Zhou, M.H. Kim, D. Banerjee, Y. Wu, F. Costanzo, I.T. Ozbolat, Aspiration-assisted freeform bioprinting of prefabricated tissue spheroids in a yield-stress gel, Commun Phys 3 (2020). https://doi.org/10.1038/s42005-020-00449-4.
[77] L. Peng, A. Chandrakar, G. Nilsson Hall, K. Ioannidis, L. Moroni, P. Wieringa, I. Papantoniou, Structurally defined cartilaginous MEW-assembloids for critical-size long bone healing, Biomaterials 319 (2025) 123202. https://doi.org/10.1016/j.biomaterials.2025.123202.
[78] R. Burdis, F. Chariyev-Prinz, D. C. Browe, F. E. Freeman, J. Nulty, E. E. McDonnell, K. F. Eichholz, B. Wang, P. Brama, D. J. Kelly, Spatial patterning of phenotypically distinct microtissues to engineer osteochondral grafts for biological joint resurfacing, Biomaterials 289 (2022) 121750. https://doi.org/10.1016/j.biomaterials.2022.121750.
[79] M. Kotlarz, C. O'Keeffe, G. S. Kronemberger, R. Burdis, S. Rana, N. Rodriguez, M. Bonizzi, P. Brama, D.J. Kelly, Biofabrication and in vivo evaluation of a hybrid osteochondral implant consisting of structurally organised engineered cartilage on a 3D-printed metal scaffold, Biomaterials 327 (2026) 123788. https://doi.org/10.1016/j.biomaterials.2025.123788.